Dynamic correlations in lipid bilayer membranes over finite time intervals

Rafael L. Schoch,[1, a)] Gilad Haran,[1, b)] and Frank L. H. Brown[2, 3, c)]
[1)]*Department of Chemical and Biological Physics, Weizmann Institute of Science, Rehovot 7610001, Israel*
[2)]*Department of Chemistry and Biochemistry, University of California, Santa Barbara, California 93106, USA*
[3)]*Department of Physics, University of California, Santa Barbara, California 93106, USA*

Recent single-molecule measurements [Schoch et. al., Proc. Nat. Acad. Sci. (USA), 118, e2113202118, 2021] have observed dynamic lipid-lipid correlations in membranes with submicron spatial resolution and submillisecond temoporal resolution. While short from an instrumentation standpoint, these length and time scales remain long compared to microscopic molecular motions. Theoretical expressions are derived to infer experimentally measurable correlations from the two-body diffusion matrix appropriate for membrane-bound bodies coupled by hydrodynamic interactions. The temporal (and associated spatial) averaging resulting from finite acquisition times has the effect of washing out correlations as compared to naive predictions (*i.e.*, the bare elements of the diffusion matrix), which would be expected to hold for instantaneous measurements. The theoretical predictions are shown to be in excellent agreement with Brownian Dynamics simulations of experimental measurements. Numerical results suggest that the experimental measurement of membrane protein diffusion, in complement to lipid diffusion measurements, might help to resolve the experimental ambiguities encountered for certain black lipid membranes.

I. INTRODUCTION

Singer and Nicholson[1] popularized the "fluid mosaic" picture of biological membranes some fifty years ago. The basic theoretical description quantifying these ideas into a hydrodynamic model was provided just a few years later by Saffman and Delbruck[2,3]. The Saffman-Delbruck (SD) model supposes the membrane to be a flat, thin, structureless, and homogeneous viscous sheet coupled on both sides to a bulk fluid via no-slip boundary conditions. Traditionally, the SD membrane is also considered to be infinitely large, with the surrounding fluid extending infinitely far to either side. However, *many* extensions of the traditional SD model have been proposed to allow for the hydrodynamic description of supported membranes[4–7], membrane vesicles[8], simulated membranes under periodic boundary conditions[9], membranes decorated with immobile inclusions[10] and membranes including an explicit representation of both monolayer leaflets in the bilayer structure[8,11,12].

SD theory was originally formulated to predict the self-diffusion coefficients of integral membrane proteins[2]. For years, it was generally accepted that this prediction (and its extension to larger diffusing bodies[13]) was a success[14,15]. However, more recent studies are divided; some authors claim significant deviations between experiment and SD-predicted diffusion coefficients[16–19], while other authors find no such disparities[20–23]. Various theoretical models have been proposed[24–29] to explain how deviations between SD theory and experiment in the self-diffusion of membrane proteins might arise. However, it is worth emphasizing that the application of hydrodynamic theories down to molecular scales (as in the prediction of self-diffusion coefficients for a single protein) is always fraught with danger and ambiguities. For example, the relevant "hydrodynamic radius" and/or boundary conditions associated with the diffusing molecule are difficult to predict from first principles, even in the case of simple molecules or globular proteins in a traditional bulk solvent[30,31]. Additional complications arise in the case of membrane systems[24–29], so perhaps it is not surprising that hydrodynamic predictions for membrane-protein self-diffusion can be problematic.

The hydrodynamic picture for membrane dynamics (SD and its many extensions) has more far-reaching implications than the prediction of self-diffusion coefficients. All dynamics at the membrane surface will be affected by hydrodynamic flows. This includes, for example, the formation, fluctuations, motion and coarsening of lipid domains[23,32–37], the rates of chemical reactions involving membrane associated reactants[38] and the influence of embedded protein inclusions on dynamics within the membrane[10,39–42]. Therefore, it is important to test hydrodynamic predictions using measurements that are well-suited to the task, as opposed to simply recognizing that self-diffusion measurements may not be adequate to fully validate hydrodynamic models.

Hydrodynamics is a continuum theory and it is best tested over distances far exceeding the molecular scale. In recent work[43], we measured dynamic correlations between well-separated (hundreds of nanometers) lipids using a single-molecule implementation of two-particle microrheology[44–46]. In principle, under ideal circumstances, these measurements would provide a direct measurement of the two-body lipid-lipid diffusion matrix, which is related to the hydrodynamic mobility matrix through a simple factor of temperature[47,48]. In the far field, off-diagonal elements of the mobility matrix report the "Oseen tensor"[47,49,50] for fluid flow (*i.e.*, the Green's function for fluid velocity response to point forcing). Consequently, two-particle microrheology measurements *should* provide detailed data suitable for direct and robust comparison to hydrodynamic predictions.

[a)]Electronic mail: schochr@igbmc.fr
[b)]Electronic mail: gilad.haran@weizmann.ac.il
[c)]Electronic mail: flbrown@chem.ucsb.edu

Current technical limitations preclude the simple comparison between experiment and theory outlined in the preceding paragraph[43]. Lipid positions are measured via induced fluorescence with illumination windows on the order of a millisecond. In that time, Brownian motion will likely displace a given lipid by over a hundred nanometers; these finite illumination periods result in measurements that reflect averaged lipid positions over the pulse duration. Since the elements of the lipid-lipid mobility/diffusion matrix are strongly separation dependent, the experimentally measured correlations do not reflect any specific value of the diffusion matrix. Rather, elements of the diffusion matrix over a whole range of separations are entangled within the readily available experimental observables. In Ref. 43, theoretical expressions for the measured correlations were used to fit the experimental data. A derivation and comprehensive validation of these expressions were not presented in that work. The missing derivation is provided here. The expressions presented in this work are truncated to linear order in the off-diagonal elements of the Smoluchowski operator for particle motion. This is expected to be a good approximation for well-separated particles, but a poor approximation for particles that approach each other very closely. For experimentally relevant cases and parameter regimes, the approximation turns out to be very accurate. Validation of this fact is provided by direct comparison to Brownian Dynamics simulations for a number of different cases. The approach described in this paper should be valuable for interpreting any future two-particle microrheology experiments that are hindered by limited temporal resolution.

The organization of this paper is as follows. The following section presents a brief overview of the experimental measurements of Ref. 43, in order to introduce theoretical quantities associated with the experimental data. Section III outlines the calculation of these theoretical quantities, keeping all terms to linear order in hydrodynamic interactions. The performance of these expressions (and the linear truncation in particular) is assessed in section IV by comparison to Brownian Dynamics simulations. In section V, numerical calculations are presented to suggest that some of the experimental ambiguities encountered in Ref. 43 might be resolvable if experiments were performed to measure the diffusion of transmembrane proteins in addition to lipids. Section VI offers a brief conclusion.

II. EXPERIMENTALLY MEASURABLE CORRELATIONS

It is well known that the self-diffusion coefficient for a Brownian particle in a homogeneous environment can be inferred from its mean squared particle displacements over time interval t via[51,52]

$$2Dt = \langle \Delta x^2 \rangle = \langle \Delta y^2 \rangle. \tag{1}$$

(This paper focuses exclusively on 2D systems; $\langle \Delta z^2 \rangle$ shares the same value as its x, y counterparts in 3D systems.) The duration over which the displacement is measured is irrelevant; the mean squared displacement is proportional to the measurement time and Eq. 1 is expected to hold true regardless of t. Further, since all positions in space are physically equivalent, displacements starting anywhere are statistically identical and may be included in the averaging process. In contrast, for a particle moving in an inhomogeneous environment, where $D(\mathbf{r})$ depends on position, averaging must include only displacements initiated from the same position $\mathbf{r}$ (denoted as $\langle \ldots \rangle_{\mathbf{r}}$) and Eq. 1 makes sense only for a short interval Δt

$$2D(\mathbf{r})\Delta t = \langle \Delta x^2 \rangle_{\mathbf{r}} = \langle \Delta y^2 \rangle_{\mathbf{r}}. \tag{2}$$

Δt has to be short enough to guarantee that the particle's random explorations do not lead to significant variations in $D(\mathbf{r})$. Equivalently, the correlations indicated in Eq. 2 are given by $2D(\mathbf{r})\Delta t$ only to lowest order in Δt.

The correlated diffusion between multiple hydrodynamically-coupled Brownian particles follows as an extension of Eq. 2[47,53]. In the specific case of two identical and disk-like lipids/proteins with cylindrical symmetry in a membrane, the distinct and nonzero elements of the diffusion matrix, $\mathbf{D}(\mathbf{r}_1, \mathbf{r}_2)$, are[39,54]

$$\begin{aligned} 2Dt &= \langle \Delta x_1^2 \rangle = \langle \Delta x_2^2 \rangle = \langle \Delta y_1^2 \rangle = \langle \Delta y_2^2 \rangle \\ 2D_c^L(A)\Delta t &= \langle \Delta x_1 \Delta x_2 \rangle_{(A,0)} \\ 2D_c^T(A)\Delta t &= \langle \Delta y_1 \Delta y_2 \rangle_{(A,0)}. \end{aligned} \tag{3}$$

These equations adopt the convention that the starting position of particle 1 defines the origin, that the vector initially separating the two particles coincides with the x axis, and that A is the magnitude of this separation (see Fig. 1). The $(A, 0)$ subscript then specifies that averaging to determine longitudinal (L, along the particle separation vector) and transverse (T, perpendicular to the separation vector) correlated diffusion coefficients is restricted to initial geometries with particle 1 at the origin and particle 2 at $(A, 0)$. There is no loss of generality in this description for a homogeneous membrane. Any pair of particles can be translated and rotated to satisfy the adopted convention without altering physical behavior. The magnitudes of $D_c^L(A)$ and $D_c^T(A)$ depend only upon the scalar separation of the particles and Eq. 9 (see below) provides a general representation of $\mathbf{D}(\mathbf{r}_1, \mathbf{r}_2)$ in terms of D, D_c^L and D_c^T for arbitrarily positioned particles.

In principle, the self-diffusion constant D also depends on particle separation and direction of motion, but this effect is vanishingly small for typical lipid systems, unless the particles are practically colliding with one another[54]. Experimentally, A is

of the order of $20\ \mathrm{nm}$ or larger, so D is assumed to be a true constant throughout this paper. Consequently, there is no restriction to short times or initial positioning in the first line of Eq. 3.

In principle, Eq. 3 offers a clear prescription for the determination of D, $D_c^L(A)$ and $D_c^T(A)$ from measured particle trajectories. In practice experimentally, only D is readily determined from these equations. Both the smallness condition on Δt and the precise determination of particle Δx, Δy are difficult to realize experimentally, as summarized in Fig. 2. The two-color single-particle-tracking pulsed-illumination scheme introduced in Ref. 43 is constrained by the detector dead time and limitations on accumulated signal strength from single fluorophores. The resulting Δt values are approximately a millisecond (longer for black lipid membranes, shorter for supported bilayers); both bright and dark intervals contribute to this window, as illustrated in Fig. 2. Using representative numbers from Ref. 43, $D \sim 15 \times 10^{-12}\ \mathrm{m}^2/\mathrm{s}$ and $\Delta t = t_{on} + t_{off} \sim 1.5 \times 10^{-3}\ \mathrm{s}$, it is estimated that the root mean squared lipid displacement ($\sqrt{4D\Delta t}$) is $300\ \mathrm{nm}$. The elements of $\mathbf{D}(A)$ show significant variations for sub-micron separations (see Sec. IV) and it is clear that the experimentally accessible Δt values are too long for a naive application of Eq. 3 to yield reliable results for D_c^L and D_c^T.

While it is infeasible to determine D_c^L and D_c^T directly from Eq. 3, the experimental measurements do report on correlations in the motion of pairs of lipids. Mathematically, these measurable correlations correspond to:

$$\begin{array}{c} \langle (\mathbb{X}_1 - A_1)(\mathbb{X}_2 - A_2) \rangle_{(A_1,0,A_2,0)} \\ \langle \mathbb{Y}_1 \mathbb{Y}_2 \rangle_{(A_1,0,A_2,0)} \end{array} \tag{4}$$

with

$$\begin{aligned} \mathbb{X}_j &= \frac{1}{t_{on}} \int_{t_{on}+t_{off}}^{2t_{on}+t_{off}} dt x_j(t) \\ \mathbb{Y}_j &= \frac{1}{t_{on}} \int_{t_{on}+t_{off}}^{2t_{on}+t_{off}} dt y_j(t) \end{aligned} \tag{5}$$

$$\begin{aligned} A_j &= \frac{1}{t_{on}} \int_0^{t_{on}} dt x_j(t) \\ 0 &= \frac{1}{t_{on}} \int_0^{t_{on}} dt y_j(t). \end{aligned} \tag{6}$$

The $(A_1, 0, A_2, 0)$ subscript indicates that only pairs of lipids with averaged positions over the first bright interval of $(A_1, 0)$ for particle 1 and $(A_2, 0)$ for particle 2 are to be included in the averaging. This coincides with how the experiments are analyzed[43]. Lipid pairs with the same "initial" separation are rotated onto the x axis and binned together for analysis, by analogy to Eq. 3, in order to provide separation-dependent observables akin to $D_c^L(A)$ and $D_c^T(A)$.

It should be clear that A_j and $\mathbb{X}_j$ are analogous physical quantities, corresponding to the averaged x coordinate of particle j during the first and second bright intervals, respectively. (It is convenient, in order to maintain a notation symmetry between particles 1 and 2 in the following section, to retain a general A_1, even though $A_1 = 0$ is specified in Figs. 1 and 2.) However, A_j constrains the ensemble considered in the averaging of Eq. 4 in the same sense that $\mathbf{r}$ constrains the ensemble of Eq. 2. A_j is simply a parameter defining the correlation in Eq. 4, it is not a dynamical variable and the notation has been chosen to emphasize this point. The fact that the A_j constraints (and similar zero constraints in the y direction) extend over the entire interval $[0, t_{on}]$, as opposed to simply specifying the particle positions at $t = 0$, leads to theoretical complications as discussed below.

The following section details the calculation of the correlations in Eq. 4. Indeed, the primary point of this paper is to present a theoretical framework for prediction of Eq. 4 and to investigate some specific realizations of this prediction.

III. THEORY

Consider two non-interacting identical disks (or "particles") evolving via coupled Brownian motion in the x, y plane. The probability distribution for the two particles evolves via the Smoluchowski equation[47,52]

$$\frac{\partial f(\mathbf{r}_1,\mathbf{r}_2,t)}{\partial t} = (W_s + W_c) f(\mathbf{r}_1,\mathbf{r}_2,t) \tag{7}$$

$$W_s \equiv D\nabla_1^2 + D\nabla_2^2 \tag{8}$$

$$\begin{aligned} W_c &\equiv \sum_{n=1,2}\sum_{m\neq n} \frac{\partial}{\partial r_{n,\alpha}} \left(\mathbf{D}(\mathbf{r}_1,\mathbf{r}_2)\right)_{n,\alpha;m,\beta} \frac{\partial}{\partial r_{m,\beta}} \\ &= \sum_{n=1,2}\sum_{m\neq n} \frac{\partial}{\partial r_{n,\alpha}} \hat{r}_{12,\alpha} \left(D_c^L(r_{12}) - D_c^T(r_{12})\right) \hat{r}_{12,\beta} \frac{\partial}{\partial r_{m,\beta}} \\ &\quad + \sum_{n=1,2}\sum_{m\neq n} \frac{\partial}{\partial r_{n,\alpha}} D_c^T(r_{12}) \frac{\partial}{\partial r_{m,\alpha}} \end{aligned} \tag{9}$$

with the formal solution

$$f(\mathbf{r}_1,\mathbf{r}_2,t) = e^{(W_s+W_c)t} f(\mathbf{r}_1,\mathbf{r}_2,0). \tag{10}$$

Here, D is the self-diffusion coefficient for a single particle whereas $\mathbf{D}(\mathbf{r}_1,\mathbf{r}_2)$ is the full diffusion matrix for the two disks. The evolution/Smoluchowski operator has been explicitly separated into self-diffusion and coupled-diffusion components. $\mathbf{r}_j$ is the position vector for disk j in the x, y plane. $r_{12} = |\mathbf{r}_1 - \mathbf{r}_2|$ and $\hat{r}_{12} = (\mathbf{r}_1 - \mathbf{r}_2)/r_{12}$. Note that the Einstein summation convention is adopted for the Greek indices associated with Cartesian directions. There are only two independent elements of $\mathbf{D}(\mathbf{r}_1,\mathbf{r}_2)$ for the *coupled* diffusion of two identical particles with cylindrical symmetry. These elements are associated with "longitudinal" correlated diffusion along the vector separating the particles ($D_c^L(r_{12})$) and "transverse" correlated diffusion perpendicular to the separation vector ($D_c^T(r_{12})$). As the notation suggests, these correlations are separation dependent, owing to the hydrodynamic interactions that propagate through the membrane and surrounding fluid. Various hydrodynamic models for lipid bilayers will be considered in Secs. IV and V, leading to different expressions and numerical values for D, $D_c^L(r_{12})$ and $D_c^T(r_{12})$.

The goal of this section is to provide theoretical expressions for the experimentally measurable correlations (Eq. 4). For concreteness, consider the longitudinal correlation (the transverse case follows similarly):

$$\langle(\mathbb{X}_1 - A_1)(\mathbb{X}_2 - A_2)\rangle_{(A_1,0,A_2,0)} = \frac{1}{t_{on}^2}\int_{t_{on}+t_{off}}^{2t_{on}+t_{off}} dt_a dt_b \left\langle (x_1(t_a) - A_1)(x_2(t_b) - A_2)\right\rangle_{(A_1,0,A_2,0)}. \tag{11}$$

Owing to the Markovian nature of the dynamics, the two-time correlation function within the integrals can be evaluated as[52]

$$\begin{aligned} \langle(x_1(t_a) - A_1)(x_2(t_b) - A_2)\rangle_{(A_1,0,A_2,0)} &= \int d\Gamma^a \int d\Gamma^b \int d\Gamma (x_1^a - A_1) P(\Gamma^a, t_a|\Gamma^b, t_b) \times \\ &\qquad (x_2^b - A_2) P(\Gamma^b, t_b|\Gamma, t_{on}) f(\Gamma, t_{on}) \\ P(\Gamma^a, t_a|\Gamma^b, t_b) &= e^{(W_s^a + W_c^a)(t_a - t_b)} \delta(\Gamma^a - \Gamma^b). \end{aligned} \tag{12}$$

The above assumes $t_a > t_b$, but the reverse ordered case is similar. Here $\Gamma \equiv (\mathbf{r}_1,\mathbf{r}_2) = (x_1, y_1, x_2, y_2)$ represents the system's position in "phase space" to simplify notation. $f(\Gamma, t_{on})$ is the distribution of particles realized at time t_{on}, starting from the flat equilibrium distribution at time 0, $f(\Gamma, 0) = f_{eq}(\Gamma) = 1/L^4$ (for a $L \times L$ box), and constrained to satisfy Eq. 6. $P(\Gamma^a, t_a|\Gamma^b, t_b)$ terms are transition probabilities from Γ^b at t_b to Γ^a at t_a. Note that the superscripts on the diffusion operators indicate the phase space variables the operators are acting on; absence of a superscript means the operators are acting on plain Γ. Eq. 12 simplifies to

$$\langle(x_1(t_a) - A_1)(x_2(t_b) - A_2)\rangle = \int d\Gamma (x_1 - A_1) e^{(W_s+W_c)(t_a - t_b)} (x_2 - A_2) e^{(W_s+W_c)(t_b - t_{on})} f(\Gamma, t_{on}), \tag{13}$$

which can be seen by recognizing that the W_s and W_c operators are self-adjoint. The time evolution operators may thus be moved off the delta functions and onto the remaining expression without any sign changes. The remaining intermediate integrals may then be taken immediately because of the delta functions.

Calculation of $f(\Gamma, t_{on})$ is somewhat involved due to the imposed constraints (Eq. 6) and is detailed in Appendix A. The result is:

$$f(\Gamma,t_{on}) = f_0(\Gamma,t_{on}) \tag{14}$$
$$+\frac{1}{(2\pi)^4}\int_0^{t_{on}} dt' \int dk e^{-ik\cdot A}\int d\Gamma' d\Gamma'' Q_0(k/t_{on}, t_{on}-t', \Gamma, \Gamma') W_c^{'} Q_0(k/t_{on}, t', \Gamma', \Gamma'') + \ldots$$

with

$$f_0(\Gamma,t_{on}) = \prod_\alpha \frac{1}{\sqrt{4\pi D t_{on}/3}} e^{-\frac{(\Gamma_\alpha - A_\alpha)^2}{4Dt_{on}/3}} \tag{15}$$
$$Q_0(q,t,\Gamma^b,\Gamma^a) = \prod_\alpha \frac{1}{\sqrt{4\pi Dt}} \exp\left[-\frac{(\Gamma_\alpha^b-\Gamma_\alpha^a)^2}{4Dt} + \frac{iq_\alpha t(\Gamma_\alpha^a+\Gamma_\alpha^b)}{2} - \frac{q_\alpha^2 Dt^3}{12}\right]$$

where the index α runs over the four components of $\Gamma = (x_1, y_1, x_2, y_2) = (\vec{r}_1, \vec{r}_2)$, $k = (k_{x_1}, k_{y_1}, k_{x_2}, k_{y_2}) = (\vec{k}_1, \vec{k}_2)$ and $A = (A_1, 0, A_2, 0) = (\vec{A}_1, \vec{A}_2)$. The explicit terms are those necessary to calculate Eq. 11 up to first order in W_c with higher order terms in the expansion included in the dots.

The time evolution operators in Eq. 13 can be expanded in powers of W_c[48,55]

$$e^{(W_s+W_c)t} = e^{W_s t} + \int_0^t dt' e^{W_s(t-t')} W_c e^{W_s t'} + \ldots \tag{16}$$

and substituting Eqs. 14 and 16 into Eq. 11 yields the perturbation expansion for the correlations

$$\langle(\mathbb{X}_1 - A_1)(\mathbb{X}_2 - A_2)\rangle = \tag{17}$$
$$\frac{1}{t_{on}^2}\sum_{n\neq m=1}^{2}\int_{t_{on}+t_{off}}^{2t_{on}+t_{off}} dt_a \int_{t_{on}+t_{off}}^{t_a} dt_b \int d\Gamma \times$$
$$\Big\{(x_n - A_n)e^{W_s(t_a-t_b)}(x_m-A_m)e^{W_s(t_b-t_{on})} f_0(\Gamma,t_{on})$$
$$+(x_n-A_n)\int_{t_b}^{t_a} dt_1 e^{W_s(t_a-t_1)} W_c e^{W_s(t_1-t_b)}(x_m-A_m)e^{W_s(t_b-t_{on})} f_0(\Gamma,t_{on})$$
$$+(x_n-A_n)e^{W_s(t_a-t_b)}(x_m-A_m)\int_{t_{on}}^{t_b} dt_2 e^{W_s(t_b-t_2)} W_c e^{W_s(t_2-t_{on})} f_0(\Gamma,t_{on})$$
$$+\frac{1}{(2\pi)^4}\int dk e^{-ik\cdot A}(x_n-A_n)e^{W_s(t_a-t_b)}(x_m-A_m)e^{W_s(t_b-t_{on})}\int_0^{t_{on}} dt_3 \int d\Gamma' d\Gamma'' \times$$
$$Q_0(k/t_{on}, t_{on}-t_3, \Gamma, \Gamma') W_c' Q_0(k/t_{on}, t_3, \Gamma', \Gamma'') + \ldots\Big\} \tag{18}$$

A number of simplifications can be made quite quickly here. All factors of $e^{W_s\tau}$ appearing to the left of W_c (and all such factors in the first term that lacks W_c) can be replaced by a 1. This is because the Laplacians in W_s yield zero contribution upon evaluating the Γ integrals by parts. It is then seen that the first term inside the braces vanishes due to the odd integrals around $A_{n(m)}$. This makes perfect physical sense. The first term is the zeroth order contribution to the correlations and there are no inter-particle correlations in the absence of W_c. The factors of $e^{W_s\tau}$ acting directly on $f_0(\Gamma, t_{on})$ reflect simple (uncorrelated) diffusive evolution starting from a Gaussian distribution at time t_{on}. The result is a broadened Gaussian with variance $2Dt_{on}/3 + 2D\tau$ in each direction:

$$e^{W_s\tau} f_0(\Gamma,t_{on}) = \prod_\alpha \frac{1}{\sqrt{4\pi(Dt_{on}/3 + D\tau)}} e^{-\frac{(\Gamma_\alpha - A_\alpha)^2}{4(Dt_{on}/3+D\tau)}}$$
$$= f_0(\Gamma, \tau + t_{on}) \quad \text{for } \tau \geq 0. \tag{19}$$

Also, the portion to the right of W_c in the second term evaluates as:

$$e^{W_s(t_1-t_b)}(x_m - A_m)e^{W_s(t_b-t_{on})} f_0(\Gamma,t_{on}) = (x_m - A_m)\frac{Dt_{on}/3 + D(t_b-t_{on})}{Dt_{on}/3 + D(t_1-t_{on})} f_0(\Gamma,t_1). \tag{20}$$

This can be seen through expressing the factor $(x_m - A_m)$ on the LHS as a derivative with respect to x_m acting on the distribution to its right. That derivative commutes with $e^{W_s\tau}$, allowing the time propagation to continue to t_1. When the derivative is then

applied, the factor of $(x_m - A_m)$ is returned. Finally, the integrals over Γ and Γ'' in the final term may be performed using results summarized in Eq. A12 in Appendix A. The results are

$$\langle(\mathbb{X}_1 - A_1)(\mathbb{X}_2 - A_2)\rangle = \tag{21}$$

$$\frac{1}{t_{on}^2}\sum_{n\neq m=1}^{2}\int_{t_{on}+t_{off}}^{2t_{on}+t_{off}} dt_a \int_{t_{on}+t_{off}}^{t_a} dt_b \times$$

$$\Big\{\int_{t_b}^{t_a} dt_1 \int d\Gamma (x_n - A_n) W_c (x_m - A_m) \frac{Dt_{on}/3 + D(t_b - t_{on})}{Dt_{on}/3 + D(t_1 - t_{on})} f_0(\Gamma, t_1)$$

$$+ \int_{t_{on}}^{t_b} dt_2 \int d\Gamma (x_n - A_n)(x_m - A_m) W_c f_0(\Gamma, t_2)$$

$$+ \int_0^{t_{on}} dt_3 \frac{1}{(2\pi)^4} \int dk e^{-ik\cdot A} \int d\Gamma' [(x_n' - A_n) + i\frac{k_{x_n}}{t_{on}} D(t_{on} - t_3)^2][(x_m' - A_m) + i\frac{k_{x_m}}{t_{on}} D(t_{on} - t_3)^2] \times$$

$$G(k/t_{on}, t_{on} - t_3, \Gamma') W_c' G(k/t_{on}, t_3, \Gamma') + \ldots\Big\} \tag{22}$$

where

$$G(k, t, \Gamma) = \prod_\alpha e^{ik_\alpha \Gamma_\alpha t} e^{-k_\alpha^2 D t^3/3}. \tag{23}$$

The calculation may proceed from this point without making further assumptions; the general results are included in Appendix B for reference. However, the hydrodynamic models considered in this work assume the membrane to be incompressible, which yields significant simplifications. The incompressibility condition results in diffusion matrices that are divergence free[56]:

$$\frac{\partial}{\partial r_{1,\alpha}} \left(\mathbf{D}(\mathbf{r}_1, \mathbf{r}_2)\right)_{1,\alpha;2,\beta} = \frac{\partial}{\partial r_{2,\beta}} \left(\mathbf{D}(\mathbf{r}_1, \mathbf{r}_2)\right)_{1,\alpha;2,\beta} = 0. \tag{24}$$

As an immediate consequence,

$$\begin{aligned} W_c &= \sum_{n=1,2}\sum_{m\neq n} \left(\mathbf{D}(\mathbf{r}_1, \mathbf{r}_2)\right)_{n,\alpha;m,\beta} \frac{\partial}{\partial r_{n,\alpha}} \frac{\partial}{\partial r_{m,\beta}} \\ &= \sum_{n=1,2}\sum_{m\neq n} \frac{\partial}{\partial r_{n,\alpha}} \frac{\partial}{\partial r_{m,\beta}} \left(\mathbf{D}(\mathbf{r}_1, \mathbf{r}_2)\right)_{n,\alpha;m,\beta}, \end{aligned} \tag{25}$$

since the apparently missing (top line) or additional (bottom line) terms involving derivatives of $\mathbf{D}$ vanish when summed over. Furthermore, in the evaluation of phase space integrals in Eq. 21, the derivatives in Eq. 25 can be made to act to the left via integration by parts. As a consequence, the first term within braces in Eq. 21 vanishes and the second term evaluates very simply. Evaluation of the remaining final term is more tedious, but the required derivatives can be taken and the Fourier integrals evaluated. The final results are written most concisely in terms of averages over the the general zeroth order distribution valid for all positive times (see Eq. A16) :

$$\left\langle \mathcal{O}(\Gamma, t) \right\rangle_0 (t) \equiv \int d\Gamma f_0(\Gamma, t) \mathcal{O}(\Gamma, t) \tag{26}$$

$$f_0(\Gamma, t) = \prod_\alpha \frac{1}{\sqrt{2\pi\sigma^2(t)}} e^{-\frac{(\Gamma_\alpha - A_\alpha)^2}{2\sigma^2(t)}}$$

$$\sigma^2(t) = \begin{cases} \frac{2Dt^3 + 2D(t_{on}-t)^3}{3t_{on}^2} & (0 < t < t_{on}) \\ \frac{2Dt_{on}}{3} + 2D(t - t_{on}) & (t > t_{on}) \end{cases}$$

where the observable $\mathcal{O}(\Gamma, t)$ is an arbitrary function of the phase space coordinates Γ and may also contain explicit time dependence, as indicated. In this notation, we have

$$\langle(\mathbb{X}_1 - A_1)(\mathbb{X}_2 - A_2)\rangle_{(A_1,0,A_2,0)} = \tag{27}$$

$$\frac{4}{t_{on}^2} \int_{t_{on}+t_{off}}^{2t_{on}+t_{off}} dt_a \int_{t_{on}+t_{off}}^{t_a} dt_b \int_{t_{on}}^{t_b} dt \left\langle D_c^L \hat{x}_{12}^2 + D_c^T \hat{y}_{12}^2 \right\rangle_0 (t)$$

$$+ \int_0^{t_{on}} dt \frac{2t^2}{t_{on}^2} \left\langle [D_c^L - D_c^T] F_1 + D_c^T F_2 \right\rangle_0 (t) + \ldots$$

with

$$
\begin{aligned}
F_1 &= (\hat{x}_{12}\mathcal{A}_1 + \hat{y}_{12}\mathcal{B}_1)\cdot(\hat{x}_{12}\mathcal{A}_2 + \hat{y}_{12}\mathcal{B}_2) \\
F_2 &= (\mathcal{A}_1\mathcal{A}_2 + \mathcal{B}_1\mathcal{B}_2) \\
\mathcal{A}_j &= \left[\frac{(x_j - A_j)^2}{\sigma^2(t)} - \frac{D(t_{on}-t)^2}{t_{on}}\left\{\frac{(x_j-A_j)^2}{\sigma^4(t)} - \frac{1}{\sigma^2(t)}\right\}\right] \\
\mathcal{B}_j &= \left[\frac{(x_j - A_j)y_j}{\sigma^2(t)} - \frac{D(t_{on}-t)^2}{t_{on}}\frac{(x_j-A_j)y_j}{\sigma^4(t)}\right].
\end{aligned}
\tag{28}
$$

Note that $\hat{x}_{12}$ and $\hat{y}_{12}$ are the components of the dimensionless separation vector, $\hat{r}_{12}$, introduced in Eq. 9. The related expression for transverse correlations follows from an analogous calculation as

$$
\begin{aligned}
&\langle \mathbb{Y}_1\mathbb{Y}_2\rangle_{(A_1,0,A_2,0)} = \\
&\frac{4}{t_{on}^2}\int_{t_{on}+t_{off}}^{2t_{on}+t_{off}} dt_a \int_{t_{on}+t_{off}}^{t_a} dt_b \int_{t_{on}}^{t_b} dt \left\langle D_c^L \hat{y}_{12}^2 + D_c^T \hat{x}_{12}^2 \right\rangle_0 (t) \\
&+ \int_0^{t_{on}} dt \frac{2t^2}{t_{on}^2}\left\langle [D_c^L - D_c^T]\tilde{F}_1 + D_c^T \tilde{F}_2 \right\rangle_0 (t) + \ldots
\end{aligned}
\tag{29}
$$

with

$$
\begin{aligned}
\tilde{F}_1 &= \left(\hat{y}_{12}\tilde{\mathcal{A}}_1 + \hat{x}_{12}\tilde{\mathcal{B}}_1\right)\cdot\left(\hat{y}_{12}\tilde{\mathcal{A}}_2 + \hat{x}_{12}\tilde{\mathcal{B}}_2\right) \\
\tilde{F}_2 &= \left(\tilde{\mathcal{A}}_1\tilde{\mathcal{A}}_2 + \tilde{\mathcal{B}}_1\tilde{\mathcal{B}}_2\right) \\
\tilde{\mathcal{A}}_j &= \left[\frac{y_j^2}{\sigma^2(t)} - \frac{D(t_{on}-t)^2}{t_{on}}\left\{\frac{y_j^2}{\sigma^4(t)} - \frac{1}{\sigma^2(t)}\right\}\right] \\
\tilde{\mathcal{B}}_j &= \left[\frac{(x_j - A_j)y_j}{\sigma^2(t)} - \frac{D(t_{on}-t)^2}{t_{on}}\frac{(x_j-A_j)y_j}{\sigma^4(t)}\right].
\end{aligned}
\tag{30}
$$

Eqs. 26 - 30 are the main results of this paper. They provide an explicit prescription for evaluation of the experimentally measurable lipid correlations. While these expressions are algebraically complicated, the $\langle\ldots\rangle_0$ averages are simply and efficiently evaluated numerically. Compared to a direct evaluation of Eq. 4 via Brownian Dynamics simulation, the expressions derived in this section are found to be at least three orders of magnitude more efficient numerically. Multiple factors contribute to this efficiency gain. Among these factors are the automatic satisfaction of constraints from Eq. 6, the known explicit form of $f_0(\Gamma, t)$, and statistical advantages inherent to the averaged expressions in Eqs. 27 and 29. The last point relates to the fact that Eqs. 27 and 29 express the experimental correlations in terms of averages of diffusion matrix elements. Naive simulations must infer the experimental correlations directly from fluctuations. As a trivial example, if $D_c^L = D_c^T = 0$, Eqs. 27 and 29 immediately predict vanishing experimental correlations with no work at all. Determining that the experimental correlations vanish from direct simulation requires substantial sampling. In effect, the results of Eqs. 26 - 30 are partially pre-averaged, leading to significant numerical savings. Though not emphasized in this paper, the impetus for deriving Eqs. 26 - 30, was the computational expense in using direct Brownian dynamics simulations to repeatedly evaluate Eq. 4 in the fitting of hydrodynamic predictions to experimental data[43]. The results provided here greatly simply that task.

The results of this section, despite their numerical appeal, are of little use if they are inaccurate. And, it should be stressed that the results derived here are only accurate to linear order in W_c. They will eventually break down when particles closely approach one another and hydrodynamic correlations become large. Fortunately, the experiments are constrained by finite spatial resolution, which effectively precludes measuring correlations for A values much smaller than $100\,\mathrm{nm}$. While this restriction on A (Eq. 6) doesn't guarantee that two particles will never come into close proximity, problematic configurations are sufficiently rare that the predicted experimental correlations are captured well by Eqs. 26 - 30. The following section compares the present results to direct simulations and finds the theoretical predictions to be very accurate for all cases of experimental interest.

IV. VALIDATION

Numerical methods and notation

Eqs. 26 - 30 require knowledge of D, $D_c^L(r_{12})$, $D_c^T(r_{12})$, t_{on} and t_{off} as inputs to predict the measurable correlations. The time scales and experimentally tunable parameters will be specified for each example discussed below. The elements of $\mathbf{D}$ are properties of the specific membrane systems studied. Direct experimental measurements are available only for self-diffusion, D; the difficulty in measuring $D_c^{L(T)}$ directly is the primary reason why this paper exists. To compare theoretical predictions with direct simulations, a number of theoretical models for the diffusion matrix are considered below. In the simplest case, closed form analytical predictions are available. The more elaborate models, involving explicit treatment of the two opposing leaflets in lipid bilayers, require numerical calculations of the diffusion matrix. These calculations are carried out using the interfacial "regularized Stokeslet"[57,58] (RS) approach that we have introduced and used previously[12,43,54,59]. Further details will not be presented here, except to specify the relevant physical parameters used in individual examples. For comparison purposes, the $D_c^{L(T)}$ curves are included in all plots of the measured correlations presented below.

Numerical evaluation of Eqs. 27 and 29 is handled in straightforward fashion. Values of the various $\langle \ldots \rangle_0(t)$ averages are calculated at evenly spaced time points over the interval $[0, 2t_{on} + t_{off}]$ by sampling particle positions from the Gaussian distrubutions specified in Eq. 26. The indicated time integrals are then carried out using the extended trapezoid rule[60].

Brownian Dynamics with hydrodynamic interactions (BD)[53] simulations are presented below to assess the accuracy of Eqs. 26 - 30. BD simulations converge toward an exact calculation of Eq. 4 for a given choice of $\mathbf{D}$; any disparities between Eqs. 27 and 29 and their analogs computed via BD indicate shortcomings of the approximations introduced in the previous section. The BD simulations reported here require various different two-particle diffusion matrices ($\mathbf{D}$) appropriate to the tangential motion of particles on membrane surfaces, as introduced below. The presented correlation curves (e.g., Fig. 3) required sampling tens of millions of two-particle trajectories to obtain the indicated error bars. Initial particle positions were sampled from a uniform distribution in space and were allowed to evolve without imposition of periodic boundary conditions, consistent with experiment. Further details related to our implementation of the BD simulations can be found in the supplemental information of Ref. 43.

To simplify the comparison of results, the measurable correlations will be presented as

$$\begin{aligned} B_c^L(A) &\equiv \frac{\langle \mathbb{X}_1(\mathbb{X}_2 - A)\rangle_{(0,0,A,0)}\big|_{\mathrm{BD}}}{2[t_{off} + t_{on}]} \\ B_c^T(A) &\equiv \frac{\langle \mathbb{Y}_1\mathbb{Y}_2\rangle_{(0,0,A,0)}\big|_{\mathrm{BD}}}{2[t_{off} + t_{on}]} \end{aligned} \tag{31}$$

$$\begin{aligned} C_c^L(A) &\equiv \frac{\langle \mathbb{X}_1(\mathbb{X}_2 - A)\rangle_{(0,0,A,0)}\big|_{\mathrm{lin}}}{2[t_{off} + t_{on}]} \\ C_c^T(A) &\equiv \frac{\langle \mathbb{Y}_1\mathbb{Y}_2\rangle_{(0,0,A,0)}\big|_{\mathrm{lin}}}{2[t_{off} + t_{on}]}. \end{aligned} \tag{32}$$

The "B" quantities correspond to correlations evaluated via full Brownian Dynamics, whereas the "C" quantities report on the linearized approximate results presented in Eqs. 26 - 30. $B_c^L(A) = D_c^L(r_{12})$ in the limit of $t_{on} \to 0$ and small t_{off}. This is because the BD simulations are numerically exact (assuming infinite sampling) and the correlation functions in Eq. 31 reduce to Eq. 3 in this limit. Also, $C_c^L(A) = D_c^L(A)$ in the same limit, as is seen by evaluating Eq. 27. The corresponding equivalences hold true for the transverse correlations. Plotting the B and C quantities in Eqs. 31 and 32 allows for a meaningful direct comparison between $D_c^{L(T)}$, $B_c^{L(T)}$ and $C_c^{L(T)}$ on the same set of axes. From the experimental perspective, one would like to be able to extract $D_c^{L(T)}$ directly from measured correlations (Eq. 4). However, naively dividing the measured correlations by $2\Delta t = 2[t_{off} + t_{on}]$ only yields correlated diffusion coefficients if the bright and dark intervals are sufficiently short. As the following examples demonstrate, experimental time scales are not sufficiently short for this naive form of data analysis to succeed. The examples will demonstrate that Eqs. 26 - 30 provide an accurate alternative to direct BD simulations, which serves as a justification for the analysis of experimental data in Ref. 43.

Certain parameters are common to most of the presented simulations/numerics and are collected in table I for reference. The remaining parameters are variable across the different examples and are detailed in the text and figures.

A. Traditional Saffman-Delbruck membrane

For a membrane treated as a single viscous sheet immersed in an infinite bath of surrounding solvent, the bilayer surface viscosity $\eta_b = 2\eta_m$ (twice the monolayer surface viscosity) and solvent viscosity η_f completely characterize membrane

Parameters		
parameter	value	meaning
r_0	0.5 nm	particle radius
η_m	1.6×10^{-10} Pa s m	monolayer viscosity
η_f	0.001 Pa s	bulk water viscosity
b	varies	inter-leaflet friction coefficient
η_f^-	varies	trapped water viscosity for supported bilayers
h	1.0 nm	separation from support for supported bilayers
t_{on}	varies	duration of bright pulses
t_{off}	varies	separation between bright pulses

TABLE I. Generic lipid bilayer properties adopted in this work. Unless specified otherwise, the following examples and figures use these values for physical parameters.

dynamics[2,3]. From a physical perspective, this model is well-suited to studying the motion of bodies that span the entire membrane (e.g., transmembrane integral proteins or membrane-spanning peptides). By symmetry, an upright cylinder spanning both leaflets will induce identical flows in both leaflets as it is forced; there is no need to consider inter-leaflet slip, as in the more elaborate models introduced below for studying the motion of lipids or other monotopic bodies.

Theoretical expressions are commonly presented in terms of the Saffman-Delbruck length $l_{SD} \equiv \eta_b/2\eta_f = \eta_m/\eta_f = 160$ nm, which marks the crossover between regimes of 2D dominated hydrodynamics within the membrane sheet itself (at short scales) and 3D dominated hydrodynamics in the solvent surrounding the sheet (at long scales)[3,4]. (It should be noted that experimental measurements of η_m vary widely, depending on the technique used, even for identical lipid systems[61]. The number chosen here is motivated by our prior investigations, based on lipid diffusion[43,59], and is on the lower end of numbers reported in the literature.) The elements of the diffusion matrix are[39,62]

$$\begin{aligned} D &= \frac{k_B T}{4\pi\eta_b}\left(\ln\frac{2l_{SD}}{r_0} - \gamma_e\right) \\ D_c^L(A) &= \frac{k_B T}{4\eta_b}\left[\frac{H_1(\tilde{r}) - Y_1(\tilde{r})}{\tilde{r}} - \frac{2}{\pi\tilde{r}^2} - \frac{r_0^2}{\pi A^2}\right] \\ D_c^T(A) &= \frac{k_B T}{4\eta_b}\left[H_0(\tilde{r}) - \frac{H_1(\tilde{r})}{\tilde{r}} - \frac{1}{2}\left(Y_0(\tilde{r}) - Y_2(\tilde{r})\right) + \frac{2}{\pi\tilde{r}^2} + \frac{r_0^2}{\pi A^2}\right] \end{aligned} \tag{33}$$

where $\tilde{r} \equiv A/l_{SD}$ is the dimensionless particle-particle separation, r_0 is the radius of the particles (assumed identical), and $\gamma_e \simeq 0.58$ is the Euler-Mascheroni constant. H_ν and Y_ν are Struve functions and Bessel functions of the second kind, respectively. These expressions assume $r_0 \ll l_{SD}$, however it should be noted that $D_c^{L(T)}$ contain leading corrections in r_0/A to the point-particle Kirkwood-like approximation that would simply involve the membrane Oseen tensor[4,63].

Fig. 3 compares $D_c^{L(T)}$, $B_c^{L(T)}$ and $C_c^{L(T)}$ for the traditional SD membrane case, using parameters from table I. (The self-diffusion coefficient is $D = 6.0\ \mu m^2/s$.) Correlation calculations were performed for three different displacement time intervals Δt, i.e., $\Delta t = 200\ \mu s$ (with $\Delta t_{on} = 100\ \mu s$ and $\Delta t_{off} = 100\ \mu s$), $\Delta t = 500\ \mu s$ (with $\Delta t_{on} = 300\ \mu s$ and $\Delta t_{off} = 200\ \mu s$), and $\Delta t = 1500\ \mu s$ (with $\Delta t_{on} = 1300\ \mu s$ and $\Delta t_{off} = 200\ \mu s$).

There are two main points to take away from Fig. 3. First, finite measurement times (Δt), lead to significant deviations between the bare correlated diffusion elements and their measurable counterparts, especially at small separations. The disparity gets more pronounced as t_{on} and t_{off} are increased. Second, the linearized results ($C_c^{L(T)}$) reproduce the BD simultions ($B_c^{L(T)}$) to within error bars; the two curves are nearly indistinguishable.

The linearized treatment of W_c in Sec. III breaks down at small inter-particle distances r_{12}, and is thus expected to lead to inaccurate predictions at small measured initial separations, A. It is difficult to observe this breakdown for experimentally resolvable separations, but it can be seen for small separations. Fig. 4 zooms in on one of the cases from Fig. 3, showing slight deviations in the BD predictions and linearized formalism for $A < 50$ nm.

B. Two-leaflet membranes

Attention is now turned to the motion of lipids. To realistically study the motion of lipids (or other monotopic bodies), the SD model must be generalized to explicitly account for the two opposing monolayers in the membrane. A depiction of the relevant hydrodynamic model is provided in Fig. 5, which is essentially the incompressible limit of the Seifert-Langer model[11]. We have described the interfacial RS implementation of this model to calculate elements of the diffusion matrix previously[12,43,59] and will not provide further details on the calculation of $\mathbf{D}(A)$ here.

Freely floating membranes

In traditional lipid membranes (as compared to the black lipid membranes discussed below), b is large[64–67], leading to strongly coupled leaflets. As a generic example of such a case, we consider an inter-leaflet friction coefficient of $b = 1 \cdot 10^8$ Pas/m. This leads to a lipid self-diffusion coefficient of $D = 6.9\ \mu m^2/s$ and correlated measurements as depicted in Fig. 6 for lipids in the same leaflet. Correlation calculations were again performed for three different displacement time intervals Δt, i.e., $\Delta t = 200\ \mu s$ (with $\Delta t_{on} = 100\ \mu s$ and $\Delta t_{off} = 100\ \mu s$), $\Delta t = 500\ \mu s$ (with $\Delta t_{on} = 300\ \mu s$ and $\Delta t_{off} = 200\ \mu s$), and $\Delta t = 1500\ \mu s$ (with $\Delta t_{on} = 1300\ \mu s$ and $\Delta t_{off} = 200\ \mu s$). The correlations between lipids in opposing leaflets were also calculated, but yield results indistinguishable from the intra-leaflet case, and are not explicitly presented. The present results are also very similar to those for the traditional SD membrane from Fig. 3. The present model reduces to SD when $b \to \infty$ and these results confirm that $b = 1 \cdot 10^8$ Pas/m is sufficiently large to effect the limiting regime.

In Ref. 43, experiments were carried out on black lipid membranes (BLMs) where a layer of organic co-solvent is sandwiched between the two membrane leaflets (see Fig. 5). This additional layer, separating the two leaflets, can lead to a substantial reduction in b. As a generic example of a BLM membrane, we consider $b = 1 \cdot 10^4$ Pas/m, leaving all other parameters the same. This results in a lipid self-diffusion coefficient of $D = 11.1\ \mu m^2/s$, approaching double that of the previous case where the leaflets were strongly coupled. (Proceeding from $b = \infty$ to $b = 0$ will result in an exact doubling of D.) Fig. 7 displays analogous calculations to Fig. 6, but with the BLM b value. In addition, the correlations for lipids in opposing leaflets are shown in Fig. 8. The experiments in Ref. 43 were performed with $\Delta t = 1500\ \mu s$ (with $\Delta t_{on} = 1210\ \mu s$ and $\Delta t_{off} = 290\ \mu s$) for BLMs, which is similar to the largest Δt considered here in the calculations. The disparity between intra-leaflet and inter-leaflet correlations is now quite apparent. The linearized equations continue to faithfully reproduce results of the full BD simulations in all of these cases.

Supported membranes

Supported lipid bilayers (SLBs) require, in addition to the parameters already introduced, specification of the subfluid viscosity (see Fig. 5). We first consider $\eta_f^- = \eta_f = 0.001$ Pas, corresponding to the water being unaffected by trapping in the $h = 1$ nm thick slab between membrane and support. And, $b = 1 \cdot 10^7\ Pas/m$ is assumed for the inter-leaflet friction. In this case, the self-diffusion coefficient in the distal leaflet is $D = 5.7\ \mu m^2/s$, whereas it is $D = 1.8\ \mu m^2/s$ in the proximal leaflet. Intra-leaflet correlations are plotted in Figs. 9 and 10 for the distal and proximal leaflets, respectively. Due to the screening of hydrodynamic interactions by the support, the SLB geometry requires a higher time-resolution compared to the previous examples; the considered time scales are: $\Delta t = 100\ \mu s$ (with $\Delta t_{on} = 50\ \mu s$ and $\Delta t_{off} = 50\ \mu s$), $\Delta t = 200\ \mu s$ (with $\Delta t_{on} = 100\ \mu s$ and $\Delta t_{off} = 100\ \mu s$), and $\Delta t = 500\ \mu s$ (with $\Delta t_{on} = 300\ \mu s$ and $\Delta t_{off} = 200\ \mu s$). The largest scale investigated is similar to the experimental $\Delta t = 640\ \mu s$ (with $\Delta t_{on} = 350\ \mu s$ and $\Delta t_{off} = 290\ \mu s$) in Ref. 43 for SLBs. Experimentally, more rapid pulsing is possible (relative to the BLM case) due to the proximity of the SLB to the glass support. This geometry makes it possible to image the membrane in total internal reflection mode and with a high numerical aperture objective, thus collecting more photons per unit time than in the BLM setting.[43]

An interesting feature of the supported geometry is the non-monotonic behavior of the transverse diffusion coefficient, which becomes negative at intermediate lipid-lipid separations. This curiosity has been noted previously[12,68] and results from the circulating flow pattern induced by a particle that is pushed across the bilayer surface (see ref. 12 for an explicit depiction of the flow). The presented correlation predictions suggest that it might be possible to observe this phenomenon experimentally, though the signature becomes quite weak in the measured signal as compared to that in the bare correlated diffusion coefficients. Due to the strong coupling between leaflets, the measured correlations (and bare diffusion elements) are very similar in both proximal and distal cases.

In the experiments of Refs. 43 and 59, it was found that the subfluid viscosity was substantially elevated relative to bulk water. To model this case, we consider $\eta_f^- = 1\ Pas$ (again with $b = 1 \cdot 10^7\ Pas/m$), corresponding to a subphase viscosity 1000 times larger than bulk. Here, the self-diffusion coefficients in the distal and proximal leaflets are $D = 4.5\ \mu m^2/s$ and $D = 0.03\ \mu m^2/s$, respectively. In Figs. 11 and 12, the corresponding correlations are presented. The elevated subfluid viscosity has the effect of nearly completely washing out the measurable correlations. The diffusion matrix itself does retain correlations for separations of a few tens of nanometers in the distal leaflet, but this is too short ranged to be detected in experimental measurements with realistic pulse times.

V. DIFFUSION FOR TRANSMEMBRANE PROTEINS

In Ref. 43, experiments were carried out on black lipid membranes (BLMs) formed from either *n*-decane (BLM_d) or *n*-hexadecane (BLM_h) solvent. In the case of BLM_d, the residual solvent sandwiched between the monolayers leads to a pro-

nounced reduction in b relative to traditional membranes devoid of such a solvent layer (see Fig. 5). This was inferred by fitting $C_c^{L(T)}$ to the experimental correlations using b as the independent fit parameter. (Since lipid self-diffusion (D) was also measured experimentally, a trial value of b implies an associated value of η_m through $D_{RS}(b, \eta_m) = D_{exp}$. All other physical parameters are known, leaving only a single independent unknown to be determined from the correlation curves. See the supplemental information of Ref. 43 for details of the fitting procedure.) However, for BLM_h, attempted fitting of $C_c^{L(T)}$ to experiment did not allow for determination of b (and η_m). The problem was not that the experimental correlations were inconsistent with theoretical predictions, but rather that that a large range of b values were all consistent with experiment. The problem is illustrated, from a theoretical perspective, in Fig. 13. Choosing two vastly different values for b leads to measurable lipid correlations that are nearly indistinguishable from one another. The raw elements of the diffusion matrix do deviate from one another at small separations, but these differences aren't sufficient to significantly influence the measurable correlations. The differences in the measurable correlations are smaller than experimental error bars.

The "resolution" to this parameter degeneracy issue, used in Ref 43, was to simply assume $\eta_m = 8 \cdot 10^{-11}\ Pasm$ for BLM_h, which is the value found for BLM_d. This approach implies that all differences in the dynamics between BLM_h and BLM_d are solely due do differences in b. While this may be a reasonable guess, it is only a guess. It was suggested in Ref. 43 that experimental measurement of both lipids and membrane-spanning objects (e.g. transmembrane peptides or proteins) might enable the determination of b and η_m for BLM_h. Fig. 13 illustrates that this determination will likely not be possible on the basis of measured correlations; the protein and lipid behaviors are all very similar regardless of the b, η_m pair considered. (The protein calculations in Fig. 13 were performed using single-sheet RS calculations, which can be realized by setting $b = 0$ in the two-leaflet model. $b = 0$ corresponds to completely decoupled monolayers and the top monolayer can then be identified with the traditional SD membrane, provided that both the monolayer viscosity and fluid viscosity are doubled to associate the whole bilayer with only the top leaflet. By symmetry, membrane spanning objects diffuse independently of monolayer slipping dynamics, b is irrelevant and the pertinent dynamics are fully captured by single-sheet calculations.) However, the self-diffusion of proteins is strongly dependent on the b, η_m pair considered through η_m. $D_{pro} = 10.6\ \mu m^2/s$ for the "high b" case and $D_{pro} = 7.2\ \mu m^2/s$ for the "low b" case. By construction, lipid $D = 13.3\ \mu m^2/s$ for both cases, because D was measured experimentally and serves as the constraint binding b and η_m values together, as discussed above.

In principle, the conclusions of the previous paragraph could depend upon the assumed radii of the lipids/proteins. If one doubles r_0 to the value $1.0\ \mathrm{nm}$, while retaining the values of b, η_m discussed above, there is a significant change in self-diffusion constants: $D = 11.6\ \mu m^2/s$, $D_{pro} = 6.3\ \mu m^2/s$ for the "low b" case and $D = 10.8\ \mu m^2/s$, $D_{pro} = 9.2\ \mu m^2/s$ for the "high b" case. However, the elements of $\mathbf{D}$ associated with particle correlations are nearly unaffected by particle size at all but the closest possible particle-particle separations. This means that the primary influence of a larger radius on measured correlations is the slower diffusion of the larger particles. The more slowly diffusing particles explore a smaller spatial region in Δt, leading to (slightly) less pronounced suppression in moving from raw correlations to measurable correlations as compared to the $r_0 = 0.5\ \mathrm{nm}$ case (see Fig. 13). However, the effect is small. Varying particle size (within reason) does not break the degeneracy issue associated with the measurable correlation curves.

Self-diffusion is readily measured to high precision (better than $\pm 0.5\ \mu m^2/s$ in Ref. 43). The results of the preceding paragraph suggest that experimental measurement of D_{pro} in BLM_h, when combined with the knowledge of lipid D, would allow for the determination of b and η_m. So, although correlated diffusion of transmembrane objects will not help resolve the experimental degeneracy for BLM_h noted in Ref.[43], there is every reason to believe that measuring self-diffusion of membrane spanning objects would resolve this degeneracy and lead to a full characterization (b and η_m) of the system. While this possibility is interesting from the theoretical standpoint, it must be mentioned that the experiment would likely require some care. BLMs are swollen by the incorporation of solvent. In the case of BLM_h, it is believed that the the bilayer may be 10% thicker than a bilayer without *n*-hexadecane present[69]. This raises the possibility of a hydrophobic mismatch between bilayer and protein, which could lead to consequences for protein motion that are not included in the quasi-2D modeling considered in this work. For example, if the protein causes a bulge or dimple in the membrane, there would be additional contributions to dynamics beyond those considered in this work[24–29].

VI. CONCLUSION

The purpose of this paper is threefold. First, a detailed derivation of Eqs. 26 - 30 has been presented. These equations were introduced without justification in Ref. 43. Second, the validity of Eqs. 26 - 30 for a range of membrane models, pulse durations and physical parameters has been established through comparison to Brownian Dynamics simulations. Only when particle separations become very small (comparable to lipid size), do the predictions begin to deviate from simulations. Such cases are not experimentally relevant. Finally, one unsatisfying loose end of Ref. 43 has been revisited. The calculations in this paper suggest that experimental measurements of membrane protein diffusion, when collected in concert with lipid diffusion, could allow for a more complete hydrodynamic-level characterization of membranes.

The last point is somewhat interesting, because the diffusive motion of membrane spanning proteins is independent of b, within the limitations of our modeling. This follows from symmetry. A cylindrical solid body extending through both leaflets

will impose the same flow profiles in both leaflets when it is forced tangentially to the membrane plane, since there is nothing to break the symmetry between the two leaflets. From a hydrodynamic standpoint, it is then clear that the mobility tensor (and hence the diffusion tensor) for protein motions cannot depend upon b. The monlayers don't slip against one another when they are moving in concert. From the standpoint of thermal fluctuations and diffusion, the two monolayers can move out of phase with one another, but such fluctuations are decoupled from the translation of the membrane-spanning objects.

It may seem ironic that measurement of a transport property that is independent of b, can help in the determination of b, but this follows from Eq. 33. If D_{pro} is measured, one can back out the membrane viscosity (η_b) and η_m simply follows as half that value. With η_m known, one can determine b from the lipid D measurement. $D(\eta_m, b)$ implies b as an implicit function of η_m for a known value of D. In the absence of a known value for D_{pro}, measuring D only provides $b(\eta_m)$ and additional measurements (or other information) are needed to characterize the system. Depending upon the physical regime and the resolution of experimental measurements, lipid-lipid correlations may or may not provide the necessary information to determine the b, η_m pair.

In cases where the correlations prove insufficiently discriminating, measurement of transmembrane protein motions in the same system would seem to be a viable alternative. In this context, we emphasize that $\mathrm{BLM_h}$ likely serves as a better proxy for biological membranes (that contain no additional alkane solvent) than does $\mathrm{BLM_d}$. The swelling of $\mathrm{BLM_d}$ is far larger than $\mathrm{BLM_h}$[69], so it is not surprising that $\mathrm{BLM_h}$ displays dynamic properties similar to those of a traditional membrane, while $\mathrm{BLM_d}$ has less conventional behavior[43]. Therefore, the practical degeneracy in parameter values associated with the lipid-only study of $\mathrm{BLM_h}$ is likely to be observed in traditional membrane systems when (if) it becomes possible to study them via two-color fluorescence measurements similar to those introduced in Ref.[43]. (In a giant vesicle geometry for example.)

ACKNOWLEDGMENTS

This work was supported in part by the Swiss National Science Foundation (Grants P300PA_174511 and P2BSP3_165336), the US-Israel Binational Science Foundation (Grant 2012084) and the NSF (Grant CHE-1800352). Use was made of the computational facilities administered by the UCSB Center for Scientific Computing at the CNSI and MRL (an NSF MRSEC; DMR-1720256) and purchased through NSF CNS-1725797. We thank Itay Barel for the use of his Regularized Stokeslets code. We thank Haim Diamant for helpful discussions.

Appendix A: Computing the particle distribution at the end of the first pulse

$f(\Gamma, t_{on})$ can be computed as

$$f(\Gamma, t_{on}) = \frac{\left\langle \prod_\alpha \delta\left(\frac{1}{t_{on}}\int_0^{t_{on}} dt\Gamma_\alpha(t) - A_\alpha\right)\delta(\Gamma_\alpha(t_{on}) - \Gamma_\alpha)\right\rangle}{\left\langle \prod_\alpha \delta\left(\frac{1}{t_{on}}\int_0^{t_{on}} dt\Gamma_\alpha(t) - A_\alpha\right)\right\rangle} \tag{A1}$$

$$= \frac{\left\langle \prod_\alpha \int dk_\alpha \delta(\Gamma_\alpha(t_{on}) - \Gamma_\alpha) e^{ik_\alpha\left(\frac{1}{t_{on}}\int_0^{t_{on}} dt\Gamma_\alpha(t) - A_\alpha\right)}\right\rangle}{\left\langle \prod_\alpha \int dk_\alpha e^{ik_\alpha\left(\frac{1}{t_{on}}\int_0^{t_{on}} dt\Gamma_\alpha(t) - A_\alpha\right)}\right\rangle}$$

$$= \frac{\int dk e^{-ik\cdot A}\int d\Gamma_0 Q(k/t_{on}, t_{on}, \Gamma, \Gamma^0)}{\int dk e^{-ik\cdot A}\int d\Gamma\int d\Gamma_0 Q(k/t_{on}, t_{on}, \Gamma, \Gamma^0)} \tag{A2}$$

which follows from Bayes' rule. The probability density for the system to be found at phase point Γ at time t_{on} conditioned on Eq. 6 holding true, is calculated as the joint probability density for the system to realize both Eq. 6 and $\Gamma(t_{on}) = \Gamma$ divided by the probability density to realize Eq. 6. The angular brackets indicate averaging over the stochastic process consistent with Eq. 10 and assuming the flat equilibrium distribution at $t = 0$. (Here, the $(A_1, 0, A_2, 0)$ subscript from the main paper is explicitly enforced via the delta functions.) The second line follows by introducing spectral representations for the delta functions associated with the constraints of Eq. 6. The third line simplifies notation by abbreviating $k \equiv (k_{x_1}, k_{y_1}, k_{x_2}, k_{y_2})$, $A \equiv (A_1, 0, A_2, 0)$ and introducing

$$Q(k, t, \Gamma^b, \Gamma^a) = \langle\delta(\Gamma(t) - \Gamma^b)e^{i\int_0^t d\tau k\cdot\Gamma(\tau)}\delta(\Gamma(0) - \Gamma^a)\rangle / \langle\delta(\Gamma(0) - \Gamma^a)\rangle$$
$$= P(\Gamma^b, t|\Gamma^a, 0)\left\langle e^{i\int_0^t d\tau k\cdot\Gamma(\tau)}\right\rangle_{\Gamma^b,\Gamma^a} \tag{A3}$$

where the Γ^b, Γ^a subscript indicates that only those trajectories of $\Gamma(t)$ satisfying $\Gamma(0) = \Gamma^a$ and $\Gamma(t) = \Gamma^b$ are included in the average. The division by $\langle\delta(\Gamma(0) - \Gamma^a)\rangle = f_{eq}(\Gamma^a) = 1/L^4$ provides a convenient definition for Q in the following analysis;

the factors of L^4 cancel between numerator and denominator in Eq. A2. Since the dynamics specified in Eq. 7 is Markovian, it is possible to formulate a related equation for $Q(k,t,\Gamma^b,\Gamma^a)$ via the Feynman-Kac theorem[70] (perhaps more familiar as Kubo-Anderson lineshape theory[71,72] or rate processes with dynamical disorder[73])

$$\frac{\partial Q(k,t,\Gamma^b,\Gamma^a)}{\partial t} = (W_s^b + W_c^b + ik\cdot\Gamma^b)Q(k,t,\Gamma^b,\Gamma^a) \tag{A4}$$

$$Q(k,0,\Gamma^b,\Gamma^a) = \delta(\Gamma^b - \Gamma^a) \tag{A5}$$

with the formal solution

$$Q(k,t,\Gamma^b,\Gamma^a) = e^{(W_s^b+W_c^b+ik\cdot\Gamma^b)t}\delta(\Gamma^b-\Gamma^a). \tag{A6}$$

This solution may be expanded in powers of W_c to give

$$\begin{aligned} Q(k,t,\Gamma^b,\Gamma^a) &= \left[e^{(W_s^b+ik\cdot\Gamma^b)t} + \int_0^t dt' e^{(W_s^b+ik\cdot\Gamma^b)(t-t')}W_c^b e^{(W_s^b+ik\cdot\Gamma^b)t'} + \ldots\right]\delta(\Gamma^b-\Gamma^a) \\ &= Q_0(k,t,\Gamma^b,\Gamma^a) + \int_0^t dt' \int d\Gamma' Q_0(k,t-t',\Gamma^b,\Gamma')W_c^{'}Q_0(k,t',\Gamma',\Gamma^a) + \ldots \end{aligned} \tag{A7}$$

Where Q_0 is obtained from Eq. A3 or A4 by substituting $W_c = 0$ in the dynamics. Unlike the full Q, the stochastic dynamics associated with Q_0 are Gaussian and, furthermore, the dynamics of the individual components of Γ are statistically independent of one another. This means that $Q_0(k,t,\Gamma^b,\Gamma^a)$, viewed as a weighted characteristic function of independent Gaussian processes, is fully determined from the first and second cumulants of the individual Γ components. Assuming $0 \le t_1 \le t_2 \le t$, these cumulants are readily calculated as

$$\kappa_{1,\alpha}(t_1) = \langle\Gamma_\alpha(t_1)\rangle^0_{\Gamma^b,\Gamma^a} = \frac{t_1}{t}\Gamma^b_\alpha + \frac{t-t_1}{t}\Gamma^a_\alpha \tag{A8}$$

$$\kappa_{2,\alpha}(t_2,t_1) = \left\langle(\Gamma_\alpha(t_2) - \langle\Gamma_\alpha(t_2)\rangle^0_{\Gamma^b,\Gamma^a})(\Gamma_\alpha(t_1) - \langle\Gamma_\alpha(t_1)\rangle^0_{\Gamma^b,\Gamma^a})\right\rangle^0_{\Gamma^b,\Gamma^a} = \frac{2D(t-t_2)t_1}{t},$$

with the index α specifying any one of the four Γ components (x_1, y_1, x_2, y_2). It follows that

$$\begin{aligned} Q_0(k,t,\Gamma^b,\Gamma^a) &= P_0(\Gamma^b,t|\Gamma^a,0)\left\langle e^{i\int_0^t d\tau k\cdot\Gamma(\tau)}\right\rangle^0_{\Gamma^b,\Gamma^a} \\ &= \prod_\alpha P_0(\Gamma^b_\alpha,t|\Gamma^a_\alpha,0)\left\langle e^{i\int_0^t d\tau k_\alpha\Gamma_\alpha(\tau)}\right\rangle^0_{\Gamma^b_\alpha,\Gamma^a_\alpha} \\ &= \prod_\alpha \frac{1}{\sqrt{4\pi Dt}}\exp\left[-\frac{(\Gamma^b_\alpha-\Gamma^a_\alpha)^2}{4Dt} + ik_\alpha\int_0^t d\tau\kappa_{1,\alpha}(\tau) - \frac{k_\alpha^2}{2}\int_0^t\int_0^t dt_2 dt_1\kappa_{2,\alpha}(t_2,t_1)\right] \\ &= \prod_\alpha \frac{1}{\sqrt{4\pi Dt}}\exp\left[-\frac{(\Gamma^b_\alpha-\Gamma^a_\alpha)^2}{4Dt} + \frac{ik_\alpha t(\Gamma^a_\alpha+\Gamma^b_\alpha)}{2} - \frac{k_\alpha^2 Dt^3}{12}\right] \end{aligned} \tag{A9}$$

Using Eq. A9 in Eq. A7 to evaluate Eq. A2 yields

$$\begin{aligned} f(\Gamma,t_{on}) &= f_0(\Gamma,t_{on})(1+C+\ldots) \\ &+\frac{1}{(2\pi)^4}\int_0^{t_{on}} dt'\int dk e^{-ik\cdot A}\int d\Gamma' d\Gamma'' Q_0(k/t_{on},t_{on}-t',\Gamma,\Gamma')W_c^{'}Q_0(k/t_{on},t',\Gamma',\Gamma'') + \ldots \end{aligned} \tag{A10}$$

where

$$f_0(\Gamma,t_{on}) = \prod_\alpha \frac{1}{\sqrt{4\pi Dt_{on}/3}}e^{-\frac{(\Gamma_\alpha-A_\alpha)^2}{4Dt_{on}/3}} \tag{A11}$$

is the distribution at time t_{on} due to the constraints imposed in Eq. 6 under unperturbed evolution with $W_c = 0$. (Note that this result is closely related to the distribution of polymer segments around the polymer center of mass for a Gaussian chain model[74].) The " C " term is a constant that is linear in W_c, originating from the denominator of Eq. A2. The exact value of this constant is unimportant, since it will contribute only at higher than linear order in the final expressions for the correlation function (Eq. 11); it has been omitted from the expressions in the main text. The dots all indicate terms of second and higher order.

The following integrals of Q_0 are also needed in the main text and are collected here.

$$\int d\Gamma^a Q_0(k,t,\Gamma^b,\Gamma^a) = \prod_\alpha e^{ik_\alpha \Gamma^b_\alpha t} e^{-k^2_\alpha D t^3/3} \equiv G(k,t,\Gamma^b) \tag{A12}$$

$$\int d\Gamma^b Q_0(k,t,\Gamma^b,\Gamma^a) = \prod_\alpha e^{ik_\alpha \Gamma^a_\alpha t} e^{-k^2_\alpha D t^3/3} = G(k,t,\Gamma^a)$$

$$\int d\Gamma^b (x^b_1 - A_1)(x^b_2 - A_2) Q_0(k,t,\Gamma^b,\Gamma^a) = [(x^a_1 - A_1) + ik_{x_1} D t^2][(x^a_2 - A_2) + ik_{x_2} D t^2] G(k,t,\Gamma^a)$$

As a slight extension to the above, it is possible to calculate the zeroth order distribution prior to the end of the first pulse, but still subject to the constraints in Eq. 6. This result is useful for expressing the averages derived in the body of the paper. From definition A3 it follows that Q (and Q_0) obey a property analogous to Chapman-Kolmogorov[52]:

$$Q(k,t-t_0,\Gamma^c,\Gamma^a) = \int d\Gamma^b Q(k,t-t',\Gamma^c,\Gamma^b) Q(k,t'-t_0,\Gamma^b,\Gamma^a) \tag{A13}$$

and it follows that

$$f_0(\Gamma,t) = \frac{\left\langle \prod_\alpha \delta\left(\frac{1}{t_{on}}\int_0^{t_{on}} dt \Gamma_\alpha(t) - A_\alpha\right)\delta(\Gamma_\alpha(t) - \Gamma_\alpha)\right\rangle_0}{\left\langle \prod_\alpha \delta\left(\frac{1}{t_{on}}\int_0^{t_{on}} dt \Gamma_\alpha(t) - A_\alpha\right)\right\rangle_0} \tag{A14}$$

$$= \frac{\int dk e^{-ik\cdot A}\int d\Gamma^f d\Gamma^i Q_0(k/t_{on}, t_{on}-t, \Gamma^f, \Gamma) Q_0(k/t_{on}, t, \Gamma, \Gamma^i)}{\int dk e^{-ik\cdot A}\int d\Gamma^f \int d\Gamma^i Q_0(k/t_{on}, t_{on}, \Gamma^f, \Gamma^i)} \tag{A15}$$

for $0 < t < t_{on}$. Using the integrals in Eq. A12, one arrives at

$$f_0(\Gamma,t) = \prod_\alpha \frac{1}{\sqrt{2\pi\sigma^2(t)}} e^{-\frac{(\Gamma_\alpha - A_\alpha)^2}{2\sigma^2(t)}} \tag{A16}$$

$$\sigma^2(t) = \frac{2Dt^3 + 2D(t_{on}-t)^3}{3t^2_{on}}.$$

Appendix B: Results for diffusion tensors that are not divergence-free

As explained in the main text, Eqs. 27 - 30 assume a diffusion tensor that is everywhere divergence free. Although one generally expects this condition to hold true in the Stokes limit for the exact diffusion tensor for pairs of cylindrical particles[56], the diffusion tensors used in some simulation schemes can exhibit non-zero divergence at small particle-particle separations[75]. The results of the main paper can be extended to the general case, though the calculations are tedious. The expressions are presented here for future reference.

$$\langle (\mathbb{X}_1 - A_1)(\mathbb{X}_2 - A_2)\rangle = \tag{B1}$$

$$\frac{1}{t^2_{on}} \int_{t_{on}+t_{off}}^{2t_{on}+t_{off}} dt_a \int_{t_{on}+t_{off}}^{t_a} dt_b \int_{t_b}^{t_a} dt \frac{\sigma^2(t_b)}{\sigma^2(t)} \left\langle [D^L_c - D^T_c]\left(-2\hat{x}^2_{12} + E_1\right) + D^T_c\left(-2 + E_2\right)\right\rangle_0 (t)$$

$$+ \frac{2}{t^2_{on}} \int_{t_{on}+t_{off}}^{2t_{on}+t_{off}} dt_a \int_{t_{on}+t_{off}}^{t_a} dt_b \int_{t_{on}}^{t_b} dt \left\langle [D^L_c - D^T_c]E_1 + D^T_c E_2\right\rangle_0 (t)$$

$$+ \int_0^{t_{on}} dt \left\langle [D^L_c - D^T_c]F_1 + D^T_c F_2\right\rangle_0 (t) + \ldots$$

where $\hat{\mathbf{r}}_{12} = (\hat{x}_{12}, \hat{y}_{12})$ is the unit length separation vector between particles 1 and 2) and the various terms are:

$$
\begin{aligned}
E_1 &= \frac{1}{\sigma^2(t)} \left(\sum_{n=1,2} \hat{x}_{12}(x_n - A_n)\hat{r}_{12} \cdot (\vec{r}_n - \vec{A}_n) \right) \\
E_2 &= \frac{1}{\sigma^2(t)} \left(\sum_{n=1,2} (x_n - A_n)^2) \right) \\
F_1 &= - \sum_{n=1,2} \sum_{m \neq n} (\hat{x}_{12}\mathcal{A} + \hat{y}_{12}\mathcal{C}) \cdot (\hat{x}_{12}\mathcal{B} + \hat{y}_{12}\mathcal{D}) \\
F_2 &= - \sum_{n=1,2} \sum_{m \neq n} (\mathcal{A}\mathcal{B} + \mathcal{C}\mathcal{D}) \\
\mathcal{A} &= \left[-\frac{(x_n - A_n)^2(t_{on} - t)}{\sigma^2(t)t_{on}} + \frac{D(x_n - A_n)^2(t_{on} - t)^3}{\sigma^2(t)^2 t_{on}^2} - \frac{D(t_{on} - t)^3}{\sigma^2(t)t_{on}^2} + 1 \right] \\
\mathcal{B} &= \left[-\frac{(x_m - A_m)^2 t}{\sigma^2(t)t_{on}} + \frac{D(x_m - A_m)^2(t_{on} - t)^2 t}{\sigma^2(t)^2 t_{on}^2} - \frac{D(t_{on} - t)^2 t}{\sigma^2(t)t_{on}^2} \right] \\
\mathcal{C} &= \left[-\frac{(x_n - A_n)y_n(t_{on} - t)}{\sigma^2(t)t_{on}} + \frac{D(x_n - A_n)y_n(t_{on} - t)^3}{\sigma^2(t)^2 t_{on}^2} \right] \\
\mathcal{D} &= \left[-\frac{(x_m - A_m)y_m t}{\sigma^2(t)t_{on}} + \frac{D(x_m - A_m)y_m(t_{on} - t)^2 t}{\sigma^2(t)^2 t_{on}^2} \right]
\end{aligned} \tag{B2}
$$

The related expressions for the transverse motions follow by substituting $\hat{x} \to \hat{y}$ and $(x_{n(m)} - A_{n(m)}) \to (y_{n(m)})$ in the above:

$$
\begin{aligned}
&\langle \mathbb{Y}_1 \mathbb{Y}_2 \rangle = \\
&\frac{1}{t_{on}^2} \int_{t_{on}+t_{off}}^{2t_{on}+t_{off}} dt_a \int_{t_{on}+t_{off}}^{t_a} dt_b \int_{t_b}^{t_a} dt \frac{\sigma^2(t_b)}{\sigma^2(t)} \left\langle [D_c^L - D_c^T] \left(-2\hat{y}_{12}^2 + \tilde{E}_1 \right) + D_c^T \left(-2 + \tilde{E}_2 \right) \right\rangle_0 (t) \\
&+ \frac{2}{t_{on}^2} \int_{t_{on}+t_{off}}^{2t_{on}+t_{off}} dt_a \int_{t_{on}+t_{off}}^{t_a} dt_b \int_{t_{on}}^{t_b} dt \left\langle [D_c^L - D_c^T]\tilde{E}_1 + D_c^T \tilde{E}_2 \right\rangle_0 (t) \\
&+ \int_0^{t_{on}} dt \left\langle [D_c^L - D_c^T]\tilde{F}_1 + D_c^T \tilde{F}_2 \right\rangle_0 (t) + \ldots
\end{aligned} \tag{B3}
$$

$$
\begin{aligned}
\tilde{E}_1 &= \frac{1}{\sigma^2(t)} \left(\sum_{n=1,2} \hat{y}_{12}(y_n)\hat{r}_{12} \cdot (\vec{r}_n - \vec{A}_n) \right) \\
\tilde{E}_2 &= \frac{1}{\sigma^2(t)} \left(\sum_{n=1,2} (y_n)^2 \right) \\
\tilde{F}_1 &= - \sum_{n=1,2} \sum_{m \neq n} (\hat{y}_{12}\mathcal{A}' + \hat{x}_{12}\mathcal{C}') \cdot (\hat{y}_{12}\mathcal{B}' + \hat{x}_{12}\mathcal{D}') \\
\tilde{F}_2 &= - \sum_{n=1,2} \sum_{m \neq n} (\mathcal{A}'\mathcal{B}' + \mathcal{C}'\mathcal{D}') \\
\mathcal{A}' &= \left[-\frac{(y_n)^2(t_{on} - t)}{\sigma^2(t)t_{on}} + \frac{D(y_n)^2(t_{on} - t)^3}{\sigma^2(t)^2 t_{on}^2} - \frac{D(t_{on} - t)^3}{\sigma^2(t)t_{on}^2} + 1 \right] \\
\mathcal{B}' &= \left[-\frac{(y_m)^2 t}{\sigma^2(t)t_{on}} + \frac{D(y_m)^2(t_{on} - t)^2 t}{\sigma^2(t)^2 t_{on}^2} - \frac{D(t_{on} - t)^2 t}{\sigma^2(t)t_{on}^2} \right] \\
\mathcal{C}' &= \left[-\frac{(x_n - A_n)y_n(t_{on} - t)}{\sigma^2(t)t_{on}} + \frac{D(x_n - A_n)y_n(t_{on} - t)^3}{\sigma^2(t)^2 t_{on}^2} \right] \\
\mathcal{D}' &= \left[-\frac{(x_m - A_m)y_m t}{\sigma^2(t)t_{on}} + \frac{D(x_m - A_m)y_m(t_{on} - t)^2 t}{\sigma^2(t)^2 t_{on}^2} \right]
\end{aligned} \tag{B4}
$$

It is worth mentioning that the order of the nested integrals in Eqs. B1 and B3 can be reduced via

$$\int_A^B dt_a \int_A^{t_a} dt_b \int_{t_b}^{t_a} dt f(t_b,t) = \int_A^B dt_b \left[B \int_{t_b}^B dt f(t_b,t) - t_b \int_A^{t_b} dt f(t,t_b) \right]$$
$$\int_A^B dt_a \int_A^{t_a} dt_b f(t_b) = \int_A^B dt_b (B-t_b) f(t_b) \tag{B5}$$

if this is convenient for numerical purposes.

REFERENCES

[1] S. J. Singer and G. L. Nicolson. The fluid mosaic model of the structure of cell membranes. Science, 175:720–731, 1972.

[2] P G. Saffman and M. Delbrück. Brownian motion in biological membranes. Proc. Nat. Acad. Sci. USA, 72:3111, 1975.

[3] P. G. Saffman. Brownian motion in thin sheets of viscous fluid. Journal of Fluid Mechanics, 73(4):593–602, feb 1976.

[4] D. K. Lubensky and R. E. Goldstein. Hydrodynamics of monolayer domains at the air-water interface. Phys. Fluids, 8:843–854, 1996.

[5] E. Evans and E. Sackmann. Translational and rotational drag coefficients for a disk moving in a liquid membrane associated with a rigid substrate. J. Fluid Mech., 194:553–561, 1988.

[6] J.-B. Fourner, A. Ajdari, and L. Peliti. Effective-area elasticity and tension of micromanipulated membranes. Phys. Rev. Lett., 86:4970–4973, 2001.

[7] Naomi Oppenheimer and Haim Diamant. Correlated dynamics of inclusions in a supported membrane. Physical Review E, 82(4):041912, oct 2010. ISSN 1539-3755. URL https://link.aps.org/doi/10.1103/PhysRevE.82.041912.

[8] E EVANS and A YEUNG. HIDDEN DYNAMICS IN RAPID CHANGES OF BILAYER SHAPE. CHEMISTRY AND PHYSICS OF LIPIDS, 73(1-2): 39–56, SEP 6 1994. ISSN 0009-3084.

[9] B. A. Camley, M. G. Lerner, R. W. Pastor, and F. L. H. Brown. Strong influence of periodic boundary conditions on lateral diffusion in lipid bilayer membranes. J. Chem. Phys., 143:243113, 2015.

[10] Naomi Oppenheimer and Haim Diamant. In-Plane Dynamics of Membranes with Immobile Inclusions. PHYSICAL REVIEW LETTERS, 107(25), DEC 13 2011. ISSN 0031-9007.

[11] U. Seifert and S. A. Langer. Viscous modes of fluid bilayer membranes. Europhys. Lett., 23:71–76, 1993.

[12] Brian A. Camley and Frank L. H. Brown. Diffusion of complex objects embedded in free and supported lipid bilayer membranes: role of shape anisotropy and leaflet structure. Soft Matter, 9(19):4767, apr 2013. ISSN 1744-683X. URL http://xlink.rsc.org/?DOI=c3sm00073g.

[13] B D. Hughes, B A. Pailthorpe, and L R. White. The translational and rotational drag on a cylinder moving in a membrane. J. Fluid Mech., 110:349, 1981.

[14] R. J. Cherry. Rotational and lateral diffusion of membrane proteins. Biochim. Biophys. Acta., 559:289–327, 1979.

[15] M. J. Saxton and K. Jacobson. Single particle tracking: Applications to membrane dynamics. Annual Review of Biophysics and Biomolecular Structure, 26: 373–399, 1997.

[16] Y Gambin, R Lopez-Esparza, M Reffay, E Sierecki, N S Gov, M Genest, R S Hodges, and W Urbach. Lateral mobility of proteins in liquid membranes revisited. Proceedings of the National Academy of Sciences, 103(7):2098–2102, feb 2006. ISSN 0027-8424. URL http://www.ncbi.nlm.nih.gov/pubmed/16461891http://www.pubmedcentral.nih.gov/articlerender.fcgi?artid=PMC1413751http://www.pnas.org/lookup/doi/10.1073/pnas.0511026103.

[17] Yann Gambin, Myriam Reffay, Emma Sierecki, Fabrice Homblé, Robert S. Hodges, Nir S. Gov, Nicolas Taulier, and Wladimir Urbach. Variation of the lateral mobility of transmembrane peptides with hydrophobic mismatch. The Journal of Physical Chemistry B, 114(10):3559–3566, feb 2010.

[18] Jana Kriegsmann, Ingo Gregor, Iris von der Hocht, Johann Klare, Martin Engelhard, Jörg Enderlein, and Jörg Fitter. Translational Diffusion and Interaction of a Photoreceptor and Its Cognate Transducer Observed in Giant Unilamellar Vesicles by Using Dual-Focus FCS. ChemBioChem, 10(11):1823–1829, jun 2009. ISSN 14394227. URL http://doi.wiley.com/10.1002/cbic.200900251.

[19] Clarence C. Lee and Nils O. Petersen. The Lateral Diffusion of Selectively Aggregated Peptides in Giant Unilamellar Vesicles. Biophysical Journal, 84(3): 1756–1764, mar 2003. ISSN 0006-3495. URL https://www.sciencedirect.com/science/article/pii/S0006349503749832.

[20] S. Ramadurai, A. Holt, V. Krasnikov, G. van den Bogaart, J. A. Killian, and B. Poolman. Lateral diffusion of membrane proteins. J. Am. Chem. Soc., 131: 12650–12656, 2009.

[21] Sivaramakrishnan Ramadurai, Andrea Holt, Lars V. Schäfer, Victor V. Krasnikov, Dirk T.S. Rijkers, Siewert J. Marrink, J. Antoinette Killian, and Bert Poolman. Influence of hydrophobic mismatch and amino acid composition on the lateral diffusion of transmembrane peptides. Biophysical Journal, 99(5): 1447–1454, sep 2010.

[22] Kerstin Weiß, Andreas Neef, Qui Van, Stefanie Kramer, Ingo Gregor, and Jörg Enderlein. Quantifying the Diffusion of Membrane Proteins and Peptides in Black Lipid Membranes with 2-Focus Fluorescence Correlation Spectroscopy. Biophysical Journal, 105(2):455–462, jul 2013. ISSN 00063495. URL https://www.sciencedirect.com/science/article/pii/S0006349513006760https://linkinghub.elsevier.com/retrieve/pii/S0006349513006760.

[23] P. Cicuta, Sarah L. Keller, and Sarah L. Veatch. Diffusion of liquid domains in lipid bilayer membranes. J. Phys. Chem. B, 111:3328, 2007.

[24] Ali Naji, Alex J. Levine, and P.A. Pincus. Corrections to the Saffman-Delbrück Mobility for Membrane Bound Proteins. Biophysical Journal, 93(11): L49–L51, dec 2007. ISSN 00063495. URL https://www.sciencedirect.com/science/article/pii/S0006349507716235https://linkinghub.elsevier.com/retrieve/pii/S0006349507716235.

[25] Vincent Démery and David S. Dean. Drag forces in classical fields. Physical Review Letters, 104(8):080601, feb 2010.

[26] V. Démery and D. S. Dean. Drag forces on inclusions in classical fields with dissipative dynamics. The European Physical Journal E, 32(4):377–390, aug 2010.

[27] Vincent Démery and David Lacoste. Mechanical Factors Affecting the Mobility of Membrane Proteins. In Physics of Biological Membranes, pages 191–211. Springer International Publishing, Cham, 2018. URL http://link.springer.com/10.1007/978-3-030-00630-3_8.

[28] A. Naji and F. L. H. Brown. Diffusion on ruffled membrane surfaces. J. Chem. Phys., 126:235103, 2007.

[29] E. Reister-Gottfried, S. M. Leitenberger, and U. Seifert. Hybrid simulations of lateral diffusion in fluctuating membranes. Phys. Rev. E, 75:011908, 2007.

[30] K. E. Van Holde, W. C. Johnson, and P. S. Ho. Principles of Physical Biochemistry. Prentice Hall, Upper Saddle River, New Jersey, second edition, 2006.

[31] Robert Zwanzig and Mordechai Bixon. Hydrodynamic theory of the velocity correlation function. Physical Review A, 2(5):2005–2012, nov 1970.

[32]S. L. Veatch and S. L. Keller. Separation of liquid phases in giant vesicles of ternary mixtures of phospholipid and cholesterol. Biophys. J., 85:3074–3083, 2003.
[33]Brian A. Camley and Frank L. H. Brown. Dynamic simulations of multicomponent lipid membranes over long length and time scales. Physical Review Letters, 105(14):148102, sep 2010.
[34]J. Fan, M. Sammalkorpi, and M. Haataja. Lipid microdomains: Structural correlations, fluctuations, and formation mechanisms. Phys. Rev. Lett., 104:118101, 2010.
[35]Eugene P. Petrov, Rafayel Petrosyan, and Petra Schwille. Translational and rotational diffusion of micrometer-sized solid domains in lipid membranes. Soft Matter, 8(29):7552, jul 2012. ISSN 1744-683X. URL http://xlink.rsc.org/?DOI=c2sm25796c.
[36]Brian A. Camley, Cinzia Esposito, Tobias Baumgart, and Frank L.H. Brown. Lipid bilayer domain fluctuations as a probe of membrane viscosity. Biophysical Journal, 99(6):L44–L46, sep 2010.
[37]Cynthia A. Stanich, Aurelia R. Honerkamp-Smith, Gregory Garbès Putzel, Christopher S. Warth, Andrea K. Lamprecht, Pritam Mandal, Elizabeth Mann, Thien-An D. Hua, and Sarah L. Keller. Coarsening Dynamics of Domains in Lipid Membranes. Biophysical Journal, 105(2):444–454, jul 2013. ISSN 00063495. URL https://www.sciencedirect.com/science/article/pii/S0006349513006917https://linkinghub.elsevier.com/retrieve/pii/S0006349513006917.
[38]Naomi Oppenheimer and Howard A. Stone. Effect of Hydrodynamic Interactions on Reaction Rates in Membranes. Biophysical Journal, 113(2):440–447, jul 2017. ISSN 00063495. URL https://www.sciencedirect.com/science/article/pii/S000634951730663X?via%3Dihubhttps://linkinghub.elsevier.com/retrieve/pii/S000634951730663X.
[39]Naomi Oppenheimer and Haim Diamant. Correlated Diffusion of Membrane Proteins and Their Effect on Membrane Viscosity. Biophysical Journal, 96(8):3041–3049, apr 2009. ISSN 0006-3495. URL https://www.sciencedirect.com/science/article/pii/S0006349509004214.
[40]Mark L. Henle and Alex J. Levine. Effective viscosity of a dilute suspension of membrane-bound inclusions. Physics of Fluids, 21(3):033106, mar 2009.
[41]Brian A. Camley and Frank L. H. Brown. Fluctuating hydrodynamics of multicomponent membranes with embedded proteins. The Journal of Chemical Physics, 141(7):075103, aug 2014.
[42]Brian A. Camley and Frank L. H. Brown. Motion of objects embedded in lipid bilayer membranes: Advection and effective viscosity. The Journal of Chemical Physics, 151(12):124104, sep 2019.
[43]Rafael L. Schoch, Frank L. H. Brown, and Gilad Haran. Correlated diffusion in lipid bilayers. Proceedings of the National Academy of Sciences, 118(48), nov 2021.
[44]John C. Crocker, M. T. Valentine, Eric R. Weeks, T. Gisler, P. D. Kaplan, A. G. Yodh, and D. A. Weitz. Two-Point Microrheology of Inhomogeneous Soft Materials. Physical Review Letters, 85(4):888–891, jul 2000. ISSN 0031-9007. URL https://link.aps.org/doi/10.1103/PhysRevLett.85.888.
[45]C. Cheung, Y. H. Hwang, X-l. Wu, and H. J. Choi. Diffusion of Particles in Free-Standing Liquid Films. Physical Review Letters, 76(14):2531–2534, apr 1996. ISSN 0031-9007. URL https://link.aps.org/doi/10.1103/PhysRevLett.76.2531.
[46]V. Prasad, S. A. Koehler, and Eric R. Weeks. Two-Particle Microrheology of Quasi-2D Viscous Systems. Physical Review Letters, 97(17):176001, oct 2006. ISSN 0031-9007. URL https://link.aps.org/doi/10.1103/PhysRevLett.97.176001.
[47]M. Doi and S. F. Edwards. The Theory of Polymer Dynamics. Clarendon Press, Oxford, 1986.
[48]R. Kubo, M. Toda, and N. Hashitsume. Statistical Physics II, Nonequilibrium Statistical Mechanics. Springer, Berlin, third corrected edition, 1998.
[49]J. Happel and H. Brenner. Low Reynolds number hydrodynamics. Kluwer, The Hague, The Netherlands, 1983.
[50]S. Kim and S. J. Karrila. Microhydrodynamics: Principles and Selected Applications. Dover, 2005.
[51]P. W. Atkins. Physical Chemistry. W. H. Freeman and Co., New York, fourth edition, 1990.
[52]N G. Van Kampen. Stochastic Processes in Physics and Chemistry. North Holland, third edition, 2007.
[53]D. L. Ermak and J. A. McCammon. Brownian dynamics with hydrodynamic interactions. J. Chem. Phys., 69:1352–1360, 1978.
[54]Ehsan Noruzifar, Brian A. Camley, and Frank L. H. Brown. Calculating hydrodynamic interactions for membrane-embedded objects. The Journal of Chemical Physics, 141(12):124711, sep 2014. ISSN 0021-9606. URL http://aip.scitation.org/doi/10.1063/1.4896180.
[55]R. M. Wilcox. Exponential operators and parameter differentiation in quantum physics. J. Math. Phys., 8:962–982, 1967.
[56]E. Wajnryb, P. Szymczak, and B. Cichocki. Brownian dynamics: divergence of mobility tensor. Physica A: Statistical Mechanics and its Applications, 335(3-4):339–358, apr 2004.
[57]Ricardo Cortez. The method of regularized stokeslets. SIAM Journal on Scientific Computing, 23(4):1204–1225, jan 2001.
[58]Ricardo Cortez, Lisa Fauci, and Alexei Medovikov. The method of regularized stokeslets in three dimensions: analysis, validation, and application to helical swimming. Physics of Fluids, 17(3):031504, mar 2005.
[59]Rafael L. Schoch, Itay Barel, Frank L. H. Brown, and Gilad Haran. Lipid diffusion in the distal and proximal leaflets of supported lipid bilayer membranes studied by single particle tracking. The Journal of Chemical Physics, 148(12):123333, mar 2018.
[60]W. H. Press, S. A. Teukolsky, W. T. Vetterling, and B. P. Flannery. Numerical Recipes in C. Cambridge University Press, Cambridge, 1994.
[61]Hammad A. Faizi, Rumiana Dimova, and Petia M. Vlahovska. A vesicle microrheometer for high-throughput viscosity measurements of lipid and polymer membranes. Biophysical Journal, 121(6):910–918, mar 2022.
[62]Yulia Sokolov and Haim Diamant. Many-particle mobility and diffusion tensors for objects in viscous sheets. The Journal of Chemical Physics, 149(3):034901, jul 2018.
[63]A. J. Levine and F. C. MacKintosh. Dynamics of viscoelastic membranes. Phys. Rev. E, 66:061606, 2002.
[64]Peter Jönsson, Jason P. Beech, Jonas O. Tegenfeldt, and Fredrik Höök. Mechanical behavior of a supported lipid bilayer under external shear forces. Langmuir, 25(11):6279–6286, may 2009.
[65]Seyed R. Tabaei, Jurriaan J. J. Gillissen, and Nam-Joon Cho. Probing membrane viscosity and interleaflet friction of supported lipid bilayers by tracking electrostatically adsorbed, nano-sized vesicles. Small, 12(46):6338–6344, sep 2016.
[66]R. Merkel, E. Sackmann, and E. Evans. Molecular friction and epitactic coupling between monolayers in supported bilayers. Journal de Physique, 50(12):1535–1555, 1989.
[67]Anne-Florence Bitbol, Jean-Baptiste Fournier, Miglena I Angelova, and Nicolas Puff. Dynamical membrane curvature instability controlled by intermonolayer friction. Journal of Physics: Condensed Matter, 23(28):284102, jun 2011.
[68]Naomi Oppenheimer and Haim Diamant. Correlated diffusion of membrane proteins and their effect on membrane viscosity. Biophys. J., 96:3041, 2009.
[69]Linda C. M. Gross, Andrew J. Heron, Sylvan C. Baca, and Mark I. Wallace. Determining Membrane Capacitance by Dynamic Control of Droplet Interface Bilayer Area. Langmuir, 27(23):14335–14342, dec 2011. ISSN 0743-7463. URL https://pubs.acs.org/doi/10.1021/la203081v.
[70]B. Oksendal. Stochastic Differential Equations: An Introduction with Applications. Springer, Berlin, fifth edition, 1998.
[71]P. W. Anderson, B. I. Halperin, and C. M. Varma. Anomalous low-temperature thermal properties of glasses and spin glasses. Philos. Mag., 25:1–9, 1972.
[72]R. Kubo. A stochastic theory of line-shape and relaxation. In D. TerHaar, editor, Fluctuation, Relaxation and Resonance in Magnetic Systems. Oliver and

Boyd, Edinburgh, 1962.
[73]R. Zwanzig. Rate processes with dynamical disorder. Acc. Chem. Res., 23:148–152, 1990.
[74]H. Yamakawa. Modern Theory of Polymer Solutions. Harper and Row, New York, 1971.
[75]G. Bossis and J. F. Brady. Self-diffusion of brownian particles in concentrated suspensions under shear. The Journal of Chemical Physics, 87(9):5437–5448, nov 1987.
[76]R. C. Major, J. E. Houston, M. J. McGrath, J. I. Siepmann, and X.-Y. Zhu. Viscous Water Meniscus under Nanoconfinement. Physical Review Letters, 96 (17):177803, may 2006. ISSN 0031-9007. URL https://link.aps.org/doi/10.1103/PhysRevLett.96.177803.
[77]Deborah Ortiz-Young, Hsiang-Chih Chiu, Suenne Kim, Kislon Voïtchovsky, and Elisa Riedo. The interplay between apparent viscosity and wettability in nanoconfined water. Nature Communications, 4(1):2482, dec 2013. ISSN 2041-1723. URL http://www.nature.com/articles/ncomms3482.

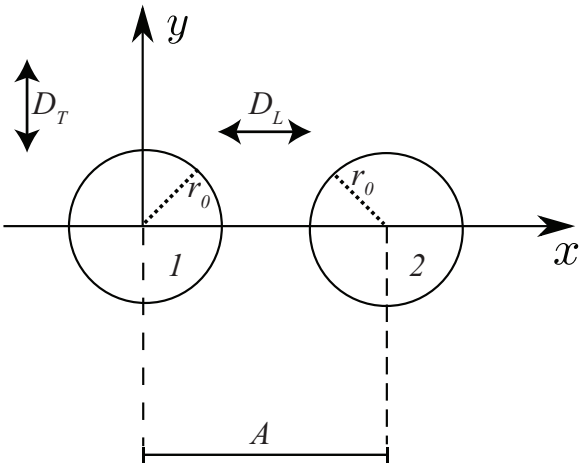

FIG. 1. Two particles separated by distance A are treated for notational convenience as lying on the x axis, with particle 1 at the origin and particle 2 at $(A, 0)$. In this convention, "longitudinal" particle motions, along the separation vector, correspond to displacements on the x axis. Displacements perpendicular to the separation vector, in the y direction, are designated as "transverse" motions. The figure is not to scale. $A \gg r_0$ for the cases studied in this work, where r_0 is the particle radius.

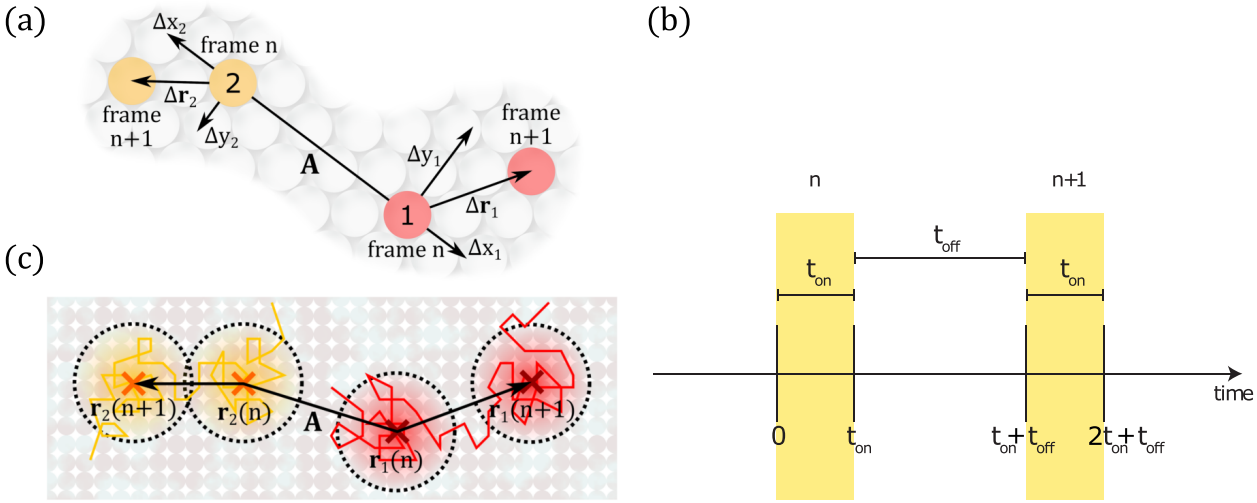

FIG. 2. Schematic of the experimental measurement of lipid correlations. (a) Theoretically, elements of the diffusion matrix can be inferred from short-time correlations in the displacement of lipids from initial (frame n) to final (frame n+1) positions via Eq. 3. (b) In practice, "initial" particle positions are collected over the entire first bright interval $[0, t_{on}]$ of the pulsed fluorescence measurement; "final" particle positions are determined over the entire second bright interval $[t_{on} + t_{off}, 2t_{on} + t_{off}]$. The inferred initial and final positions of the lipids reflect time averages of duration t_{on}, corresponding to sampling lipid positions over the bright intervals. (Experimentally, these time averages also include the localization uncertainty for single molecules, which is not explicitly considered in this work.) (c) Additionally, the lipids sample different relative positions with different $\mathbf{D}(\mathbf{r}_1, \mathbf{r}_2)$ during the entire measurement spanning $[0, 2t_{on} + t_{off}]$. Adapted from Ref. 43.

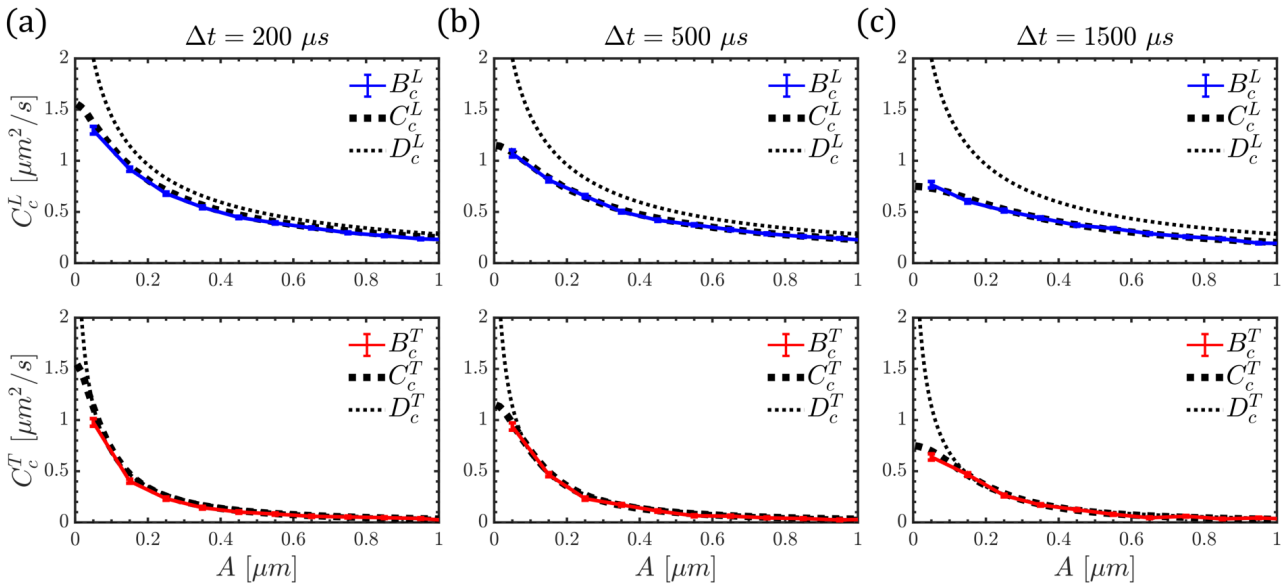

FIG. 3. Correlated diffusion in a single-sheet SD membrane. Measurable correlations obtained using the linearized formalism, $C_c^{L(T)}(A)$, and BD simulations, $B_c^{L(T)}(A)$, are compared to bare diffusion matrix elements, $D_c^{L(T)}(A)$. (a) $\Delta t = 200\ \mu s$ (with $\Delta t_{on} = 100\ \mu s$ and $\Delta t_{off} = 100\ \mu s$). (b) $\Delta t = 500\ \mu s$ (with $\Delta t_{on} = 300\ \mu s$ and $\Delta t_{off} = 200\ \mu s$). (c) $\Delta t = 1500\ \mu s$ (with $\Delta t_{on} = 1300\ \mu s$ and $\Delta t_{off} = 200\ \mu s$). Longitudinal correlations are on the top plots and transverse correlations on the bottom plots. Note that $D_c^{L(T)}(A)$ are not affected by the pulse duration. The diffusion matrix is an intrinsic property of the membrane and remains identical for all Δt values; it is included in all the plots for comparison purposes.

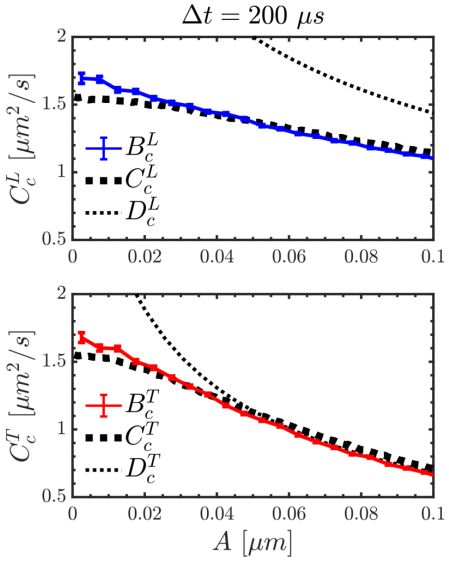

FIG. 4. Correlated diffusion in a single-sheet SD membrane at small particle separations with $\Delta t = 200\ \mu s$. The plots correspond to the leftmost case in Fig. 3, but zooming in on smaller A. The deviations between $C_c^{L(T)}(A)$ and $B_c^{L(T)}(A)$ are due to inaccuracies in the linearization approximation.

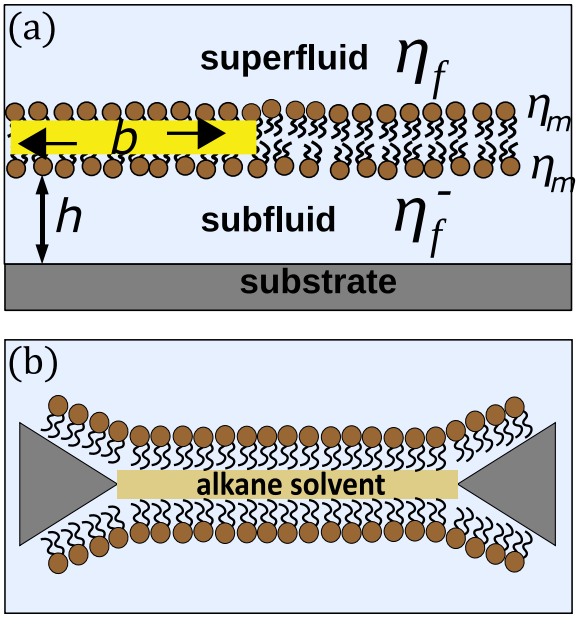

FIG. 5. Membrane model. (a) The diffusion matrix for lipids (or other monotopic bodies) in a two-leaflet membrane in the creeping flow limit depends upon: monolayer surface viscosity (η_m, both leaflets are assumed identical throughout this work), bulk fluid viscosity for the surrounding solvent (η_f) and the inter-leaflet friction coefficient (b). Additionally, if the membrane is supported by a solid substrate, it is necessary to specify the separation between the membrane and support (h) and the viscosity of the trapped water (η_f^-), which may differ substantially from the infinite bulk value[76,77]. In the case of freely floating membranes, $\eta_f^- = \eta_f$ and $h = \infty$. (b) Schematic of a black lipid membrane (BLM) with alkane co-solvent sandwiched between the two membrane leaflets, leading to reduced inter-leaflet friction as compared to a traditional lipid bilayer. The extent of membrane swelling depends upon the particular alkane used, with shorter chain alkanes typically causing more swelling than longer chain alkanes. For example, *n*-decane is believed to swell bilayers by 62% as compared to 10% sweelling by *n*-hexadecane[69].

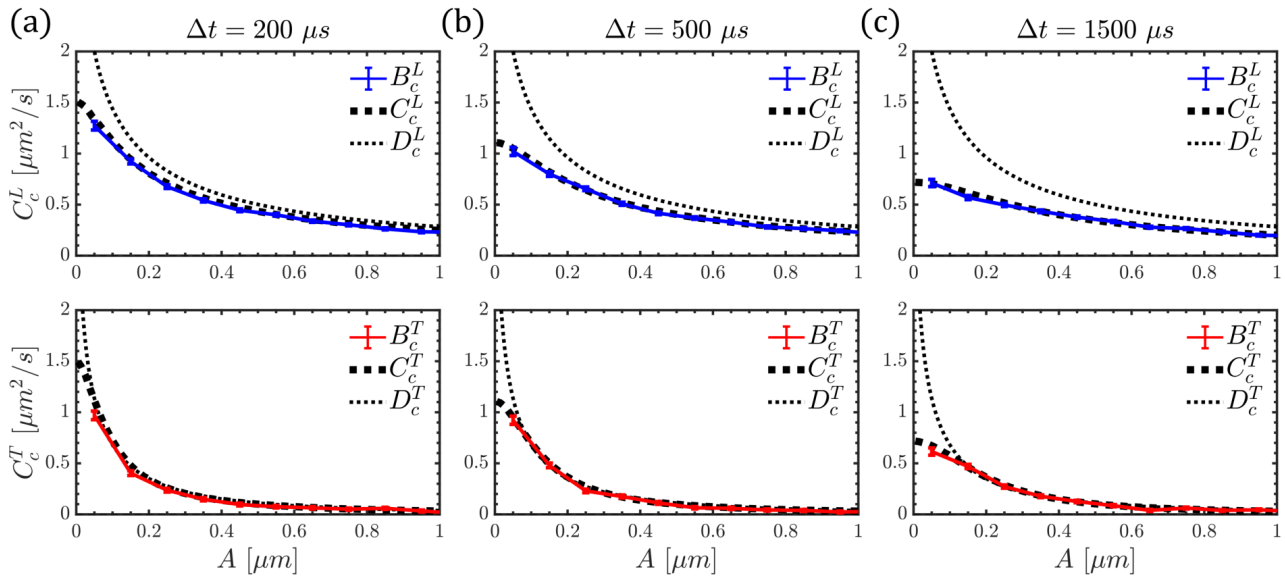

FIG. 6. Intra-leaflet correlated diffusion in a two-leaflet membrane with high inter-monolayer friction (i.e., $b = 1 \cdot 10^8\ Pas/m$). The analogous results for inter-leaflet correlations are indistinguishable from these results and are not explicitly plotted. Indeed, both the inter- and intra-leaflet correlations are essentially identical to the single-sheet SD results of Fig. 3, reflecting the tight coupling between leaflets imposed by high b values. The cases (i.e. pulsing conditions) considered here are identical to those in Fig. 3.

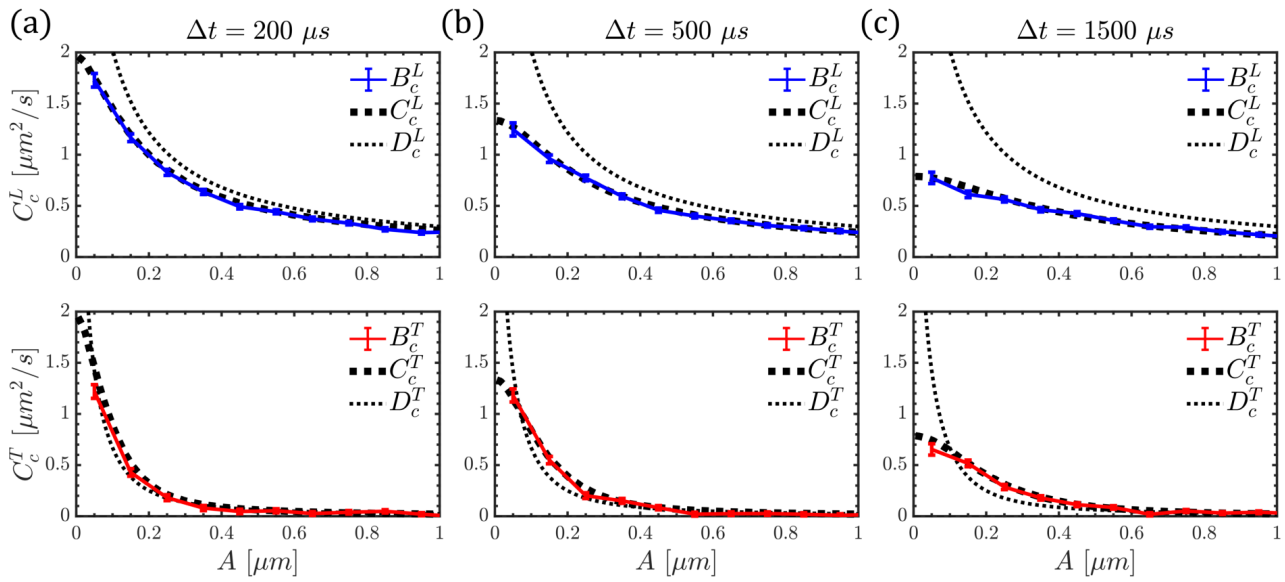

FIG. 7. Intra-leaflet correlated diffusion in a two-leaflet membrane with low inter-monolayer friction (i.e., $b = 1 \cdot 10^4\ Pas/m$). The cases considered here are identical to those in Fig. 3.

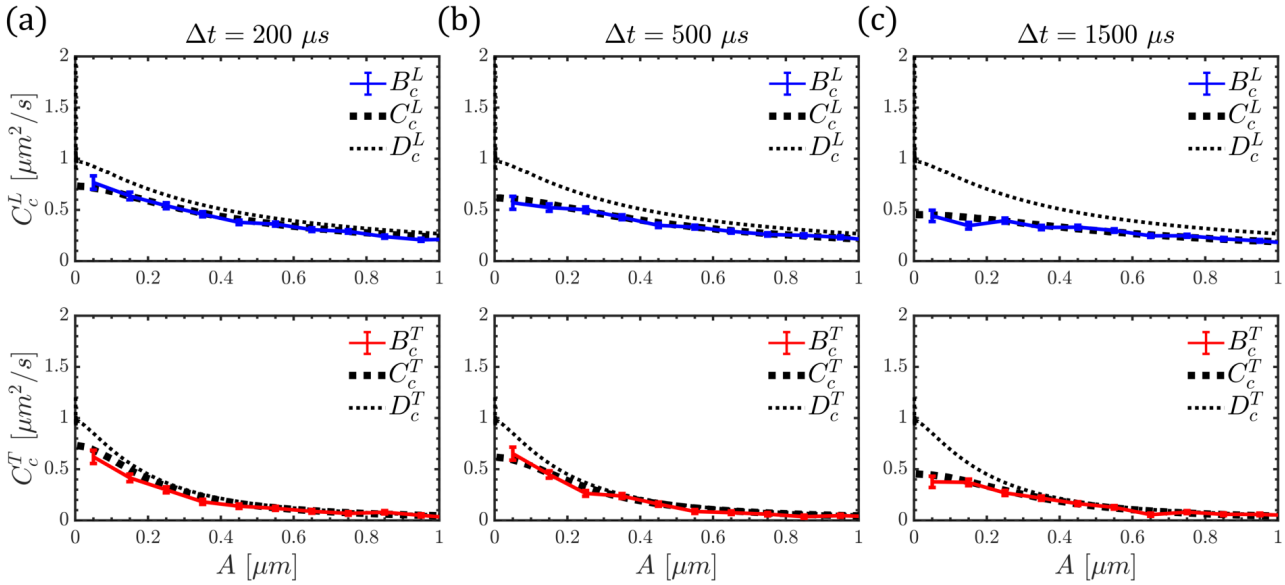

FIG. 8. Inter-leaflet correlated diffusion in a two-leaflet membrane with low inter-monolayer friction (i.e., $b = 1 \cdot 10^4\ Pas/m$). The cases considered here are identical to those in Fig. 3.

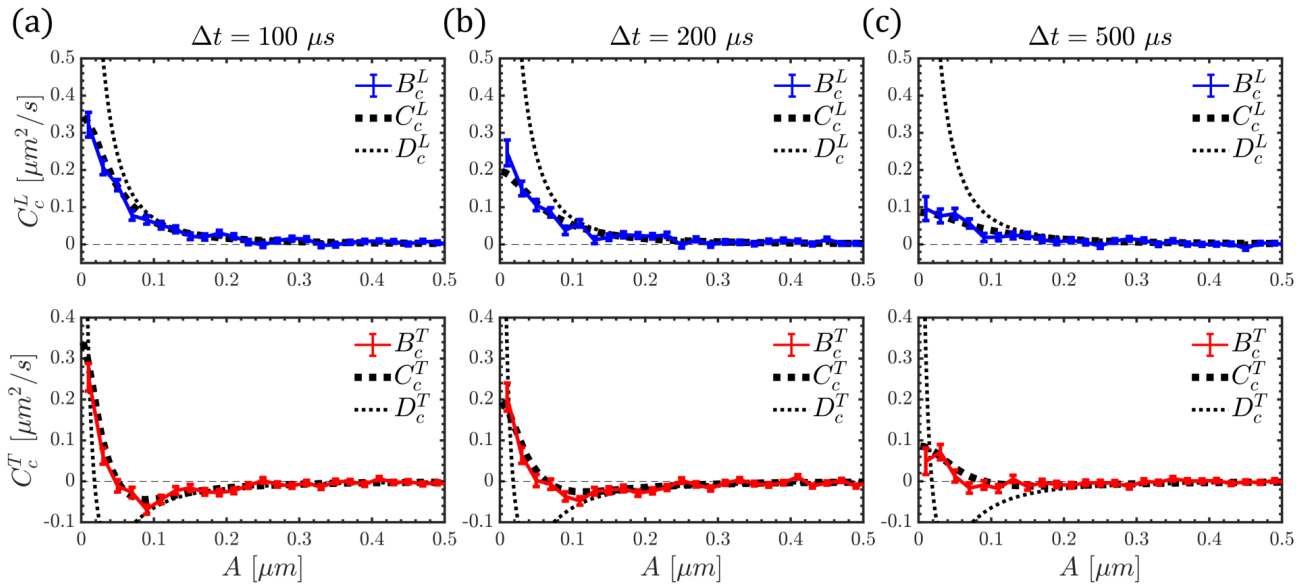

FIG. 9. Correlated diffusion in the distal leaflet of an SLB with low subphase viscosity (i.e., $\eta_f^- = 0.001\ Pas$). Measurable correlations obtained using the linearized formalism, $C_c^{L(T)}(A)$, and BD simulations, $B_c^{L(T)}(A)$, are compared to bare diffusion matrix elements, $D_c^{L(T)}(A)$. (a) $\Delta t = 100\ \mu s$ (with $\Delta t_{on} = 50\ \mu s$ and $\Delta t_{off} = 50\ \mu s$). (b) $\Delta t = 200\ \mu s$ (with $\Delta t_{on} = 100\ \mu s$ and $\Delta t_{off} = 100\ \mu s$). (c) $\Delta t = 500\ \mu s$ (with $\Delta t_{on} = 300\ \mu s$ and $\Delta t_{off} = 200\ \mu s$). Longitudinal correlations are on the top plots and transverse correlations on the bottom plots.

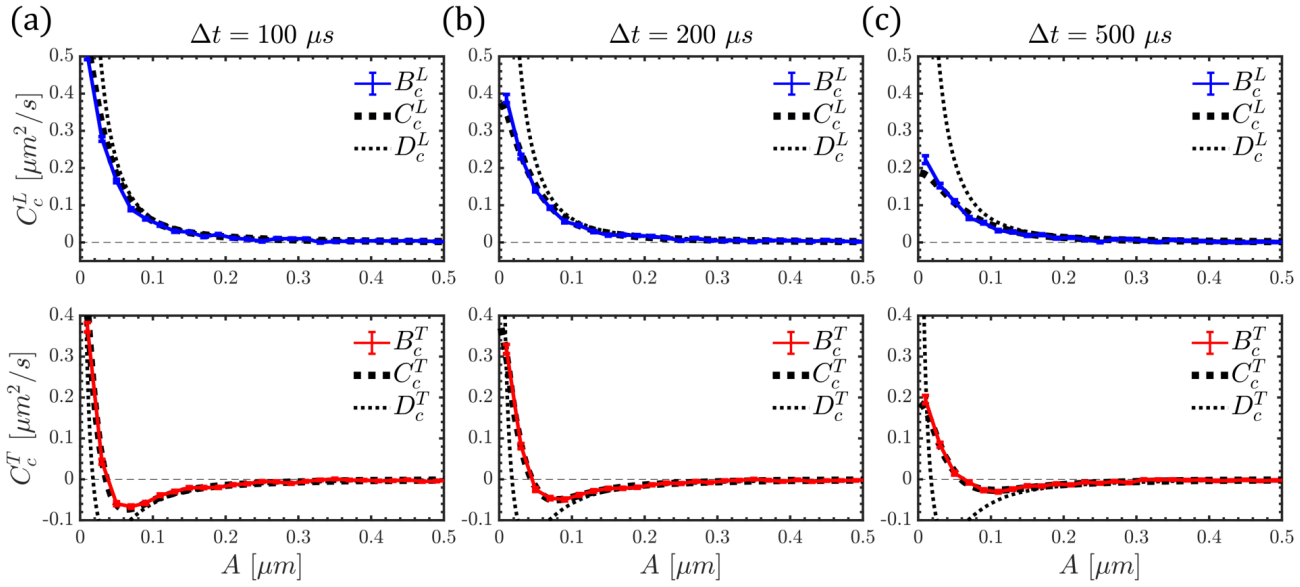

FIG. 10. Correlated diffusion in the proximal leaflet of an SLB with low subphase viscosity (i.e., $\eta_f^- = 0.001\ Pas$). The remaining parameters are identical to Fig. 9.

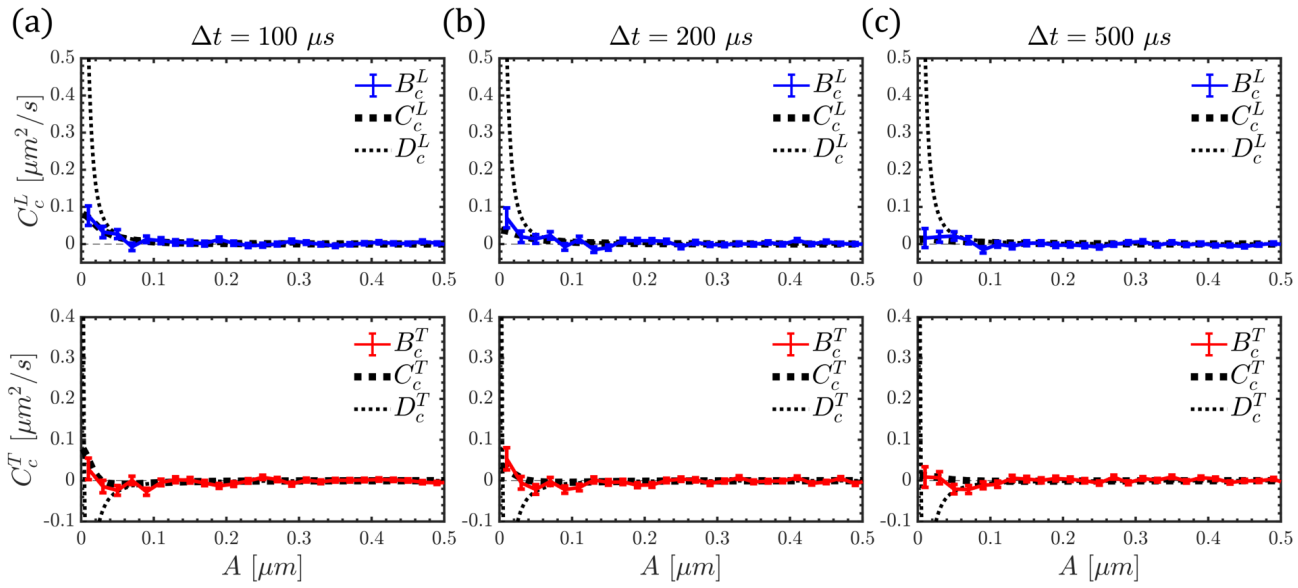

FIG. 11. Correlated diffusion in the distal leaflet of an SLB with high subphase viscosity (i.e., $\eta_f^- = 1\ Pas$). The remaining parameters are identical to Fig. 9.

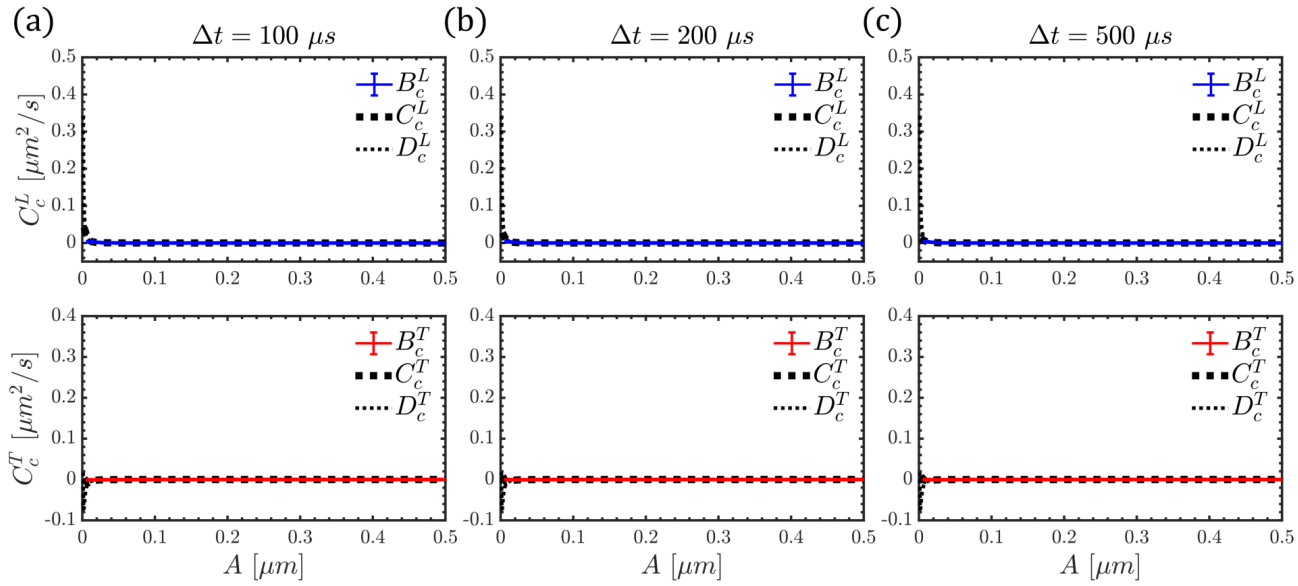

FIG. 12. Correlated diffusion in the proximal leaflet of an SLB with high subphase viscosity (i.e., $\eta_f^- = 1\ Pas$). The remaining parameters are identical to Fig. 9.

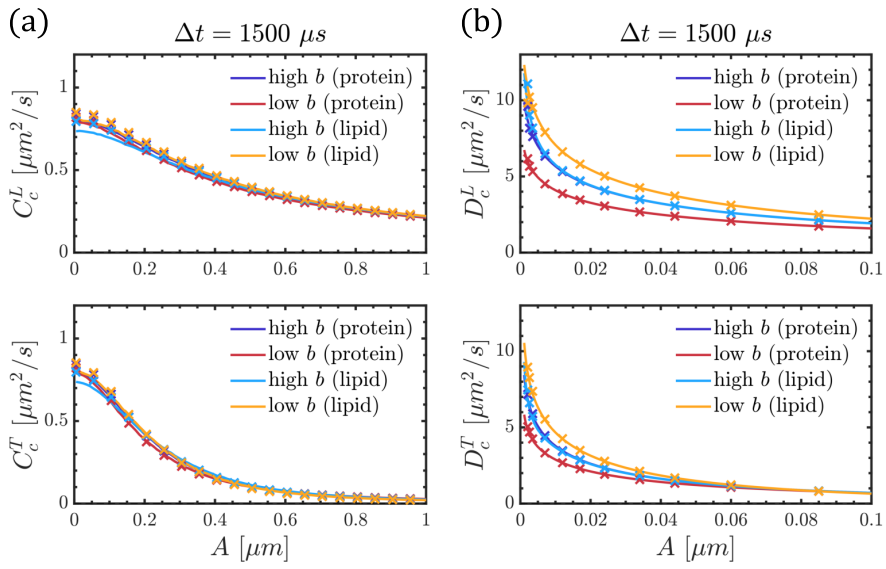

FIG. 13. Parameter degeneracy issue for the BLM_h system with $\Delta t = 1500\ \mu s$ (with $\Delta t_{on} = 1300\ \mu s$ and $\Delta t_{off} = 200\ \mu s$). (a) The predicted measurable correlations, $C_c^{L(T)}(A)$, are shown for lipids as well as transmembrane proteins of the same radius ($r_0 = 0.5$ nm, solid lines). Two different limiting cases, "high b" ($b = 1.8 \cdot 10^7\ Pas/m$) and "low b" ($b = 1 \cdot 10^4\ Pas/m$), are presented. Both cases are consistent with the experimentally measured value of $D = 13.3\ \mu m^2/s$ for the lipids when $r_0 = 0.5$ nm. The corresponding values of η_m set by this experimental constraint on D are $\eta_m = 8 \cdot 10^{-11}\ Pasm$ for the "high b" case and $\eta_m = 13 \cdot 10^{-11}\ Pasm$ for the "low b" case. The measurable correlations are essentially identical (within experimental error bars) for both cases and even for proteins as compared to lipids for the parameter regime associated with BLM_h. For comparison purposes, data for $r_0 = 1.0$ nm and the same b, η_m values from above are presented as crosses. The larger, more slowly diffusing, particles are subject to less spatial averaging and hence the correlations curves are slightly elevated relative to the $r_0 = 0.5$ nm case. However, the curves remain indistinguishable within experimental errors. Section IV has firmly established the excellent correspondence between $C_c^{L(T)}$ and $B_c^{L(T)}$; only the $C_c^{L(T)}$ curves are explicitly displayed here for clarity. (b) Regularized Stokeslet calculations for the raw diffusion matrix elements, $D_c^{L(T)}(A)$, for the different scenarios presented in (a). Note that these figures focus attention on smaller separations, where differences are most apparent. Correlated diffusion is essentially unaffected by particle radius, unless the particles are nearly contacting each other.